Tellus (2006), 58B, 257–278
Printed in Singapore. All rights reserved

TELLUS

A dynamic-flow carbon-cycle box model and high-latitude sensitivity

By EMILY LANE[1], SYNTE PEACOCK[2*] and JUAN M. RESTREPO[3], [1]*Institute of Geophysics and Planetary Physics, University of California Los Angeles, Los Angeles, CA 90095, USA;* [2]*Department of the Geophysical Sciences, University of Chicago, Chicago, IL 60637, USA;* [3]*Department of Atmospheric Sciences and Physics Department, University of Arizona, Tucson, AZ 85721, USA*

(Manuscript received 20 June 2005; in final form 19 April 2006)

ABSTRACT

Most of the hypotheses put forward to explain glacial–interglacial cycles in atmospheric pCO_2 are centred on Southern-Ocean-based mechanisms. This is in large part because: (1) timing constraints rule out changes in the North Atlantic as the trigger; (2) the concept of "high-latitude sensitivity" eliminates changes in the non-polar oceans as likely contenders. Many of the Southern-Ocean-based mechanisms for changing atmospheric pCO_2 on glacial–interglacial time-scales are based on results from highly simplified box models with prescribed flow fields and fixed particulate flux. It has been argued that box models are significantly more "high-latitude sensitive" than General Circulation Models. In light of this, it is important to understand whether this high-latitude sensitivity is a feature common to all box models, and whether the apparent degree of sensitivity changes for different tracers and parameters. We introduce a new metric for assessing how "high-latitude sensitive" a particular solution is to perturbations. With this metric, we demonstrate that a given model may be high-latitude sensitive to certain parameters but not to others. We find that the incorporation of a dynamic-based flow field and a Michaelis–Menten type nutrient feedback can have a significant impact on the apparent sensitivity of the model to perturbations. The implications of this for current box-model-based estimates of atmospheric pCO_2 drawdown are discussed.

1. Introduction

Many of the leading hypotheses which seek to explain (at least in part) the observed variations in glacial–interglacial pCO_2 derive from reduced-complexity models. The advantage of such models is that they yield solutions at effectively zero cost, thereby allowing an extensive investigation of parameter space. General Circulation Models (GCMs) are arguably more realistic, but lie at the other end of the spectrum of computational expense. Ideally, one might attempt a forward run of a fully coupled three-dimensional ocean-atmosphere GCM to study possible causes of glacial–interglacial pCO_2 changes. This, however, is still computationally infeasible, even at coarse resolution. In the absence of complete and accurate benchmarks by which to assess how much box-model-based results differ from those which GCMs would yield (given sufficient computational resources), researchers have proposed a variety of metrics. Most widely cited are Broecker's "HBEI" and Archer's "abiotic pCO_2".

Comparison of the values of these indices in different models has led to debate over the observation that box models appear to be much more sensitive to high-latitude perturbations than do GCMs (which would be expected to bear a closer resemblance to the real ocean, Archer and Winguth 2000). Because many hypotheses for the glacial–interglacial change in atmospheric pCO_2 rely on a "high-latitude sensitive" mechanism, and many more can be ruled out if the low latitudes really are a minor player, it is important to understand this apparent "sensitivity". The first step in solving the high-latitude sensitivity debate is to reach a consensus on the meaning of "high-latitude sensitivity". In assessing the degree to which a model is high-latitude sensitive, do we seek to measure the response of a specified tracer to a small change in a given parameter, do we seek an analogy for mean equilibration temperature, or do we seek to compare different model states? In what follows, we demonstrate that: (a) whether or not a model is high-latitude sensitive is not related to whether it is a box model or GCM, but rather, on how the model is constructed; (b) a given model can exhibit high-latitude sensitivity to certain parameters, but not to others; and (c) commonly used metrics such as the HBEI when applied to our model yield a range of values spanning "box-model-like" values to "GCM-like" values depending on the precise definition of the metric used.

We develop a low-dimensional box model with a dynamic flow field, and feedback between nutrient levels and particulate

*Corresponding author.
e-mail: synte@geosci.uchicago.edu
DOI: 10.1111/j.1600-0889.2006.00192.x

flux. For the purposes of this study, the term "dynamic flow" is used simply to refer to the fact that the flow is dependent on density gradients within the model (as described in Appendix A). The more conventional carbon box model, in which the flow field is prescribed a priori, and has no dependence on the density field, we term "dynamically inconsistent". We show how these changes to the model affect its sensitivity using "Linearized Sensitivity Analysis" (LSA hereafter, Cao et al., 2003). We outline several key aspects of the model derivation, particularly its hydrodynamics, in order to illustrate the fundamental difference between this box model and many of those used in the "high-latitude sensitivity" debate.

In order to rigorously compare how model behaviour changes under different parametrizations, we show how LSA can be used as a diagnostic tool with which to quantify sensitivity of model steady-state solutions. LSA is well established mathematically, generally applicable, and practical. Most importantly, one can assess how a tracer in a given region might respond differently to perturbations in various parameters. Because LSA captures the tangent linear approximation of any model with respect to parameter space, it can handle the complex coupling of the dynamics and parameters in a consistent way. The technique also yields a qualitative assessment of important and ignorable components of a model. This can be an extremely useful tool in model design, reduction and analysis.

The fluid dynamics of this box model and its dependence on the salt and heat content is designed to be consistent, to lowest order, with the analytical thermohaline circulation models explored by Cessi and Young (1992), Thual and McWilliams (1992) and Marotzke and Willebrand (1991). As such, our box model will collapse to the familiar two-box model of Stommel (1961) with symmetric forcing (see four-box model generalizations, such as those proposed by Griffies and Tziperman, 1995; Gildor and Tziperman, 2001; Shaffer and Olsen, 2001). However, unlike these box models, we capture the pole-to-pole flow asymmetry with sinking in both hemispheres that is more typical of GCMs and the modern-day ocean. As with the studies cited above, the strength of the overturning flow scales directly with the equator–pole density gradient. It should be noted that it has recently been suggested that the opposite might in fact be the case; that increasing the lateral density gradient may reduce vertical mixing, and that the net effect might in fact be a *reduction* in the overturning circulation (Nilsson et al., 2003). However, investigating such a possibility lies beyond the scope of this work.

The model we develop here has a feedback between phosphate levels and particulate flux, which is lacking in conventional carbon-cycle box models which have been applied to the glacial–interglacial atmospheric pCO_2 problem (Sarmiento and Toggweiler, 1984; Siegenthaler and Wenk, 1984; Toggweiler, 1999; Toggweiler et al., 2003). However, the model can be configured in a way similar to most conventional box models, with a prescribed flow field and fixed particulate flux. Comparisons of the dynamic-flow case versus the fixed-flow case and the fixed versus variable particulate flux allow us to infer the relative importance of flow- and nutrient-dynamics (both absent in most other carbon-cycle box models) in regulating glacial–interglacial atmospheric pCO_2.

2. A dynamic-flow model with Michaelis–Menten type feedback

There exist a number of box models of various complexity (e.g. Knox and McElroy, 1984; Sarmiento and Toggweiler, 1984; Toggweiler, 1999; Stephens and Keeling, 2000) which have been applied to the atmospheric pCO_2 problem. Most of these models share several unrealistic features. In particular, it is commonplace to specify a flow field a priori, which does not achieve dynamic consistency with the underlying density field. An identical flow field for present-day and glacial conditions is frequently assumed, despite firm evidence for changes in temperature and salinity (Beck et al., 1992; Guilderson et al., 1994; Adkins et al., 2002). These fixed-flow models we term "dynamically inconsistent" because the magnitude and direction of the flow field in the real ocean, to lowest order, depend on lateral density gradients.

Other common shortcomings of box models commonly applied to the glacial–interglacial atmospheric pCO_2 problem include the assumption of zero nutrient concentration in the non-polar surface ocean, an unrealistically low global export production, lack of feedback between export production and nutrient concentration in the upper ocean, and missing horizontal and/or vertical mixing terms. In this paper, we develop a simple carbon-cycle box model which addresses these issues. The model has a flow field based on hydrodynamics which evolves as the density structure of the model evolves; the surface-ocean nutrient concentration is not required to be identically zero; the total export production is in good agreement with observational estimates (Table 5); the biological export production incorporates a Michaelis–Menten (MM) type feedback; and all mixing terms are included between all boxes.

Our strategy in designing a model for ocean circulation on time-scales of the order of thousands of years was to construct a low-dimensional, low-frequency model with a scaling that leads to the zonally averaged *thermohaline convection* equations as derived by Thual and McWilliams (1992) and Cessi and Young (1992) (see also Marotzke and Willebrand, 1991), augmented by simplified equations for tracers, which are assumed to evolve via advection–diffusion equations. The relevance of a two-dimensional simplified model to the three-dimensional ocean is discussed in some detail in the three above-mentioned studies. Coriolis effects, topographic effects and surface wind stresses are ignored. Zonal averaging and the adoption of a simplified model for the dissipation of momentum and tracers imply tuned eddy viscosity and diffusivity parameters.

Figure 1 shows a diagram of the six-box model. There are three surface boxes representing the Southern "S", non-polar or

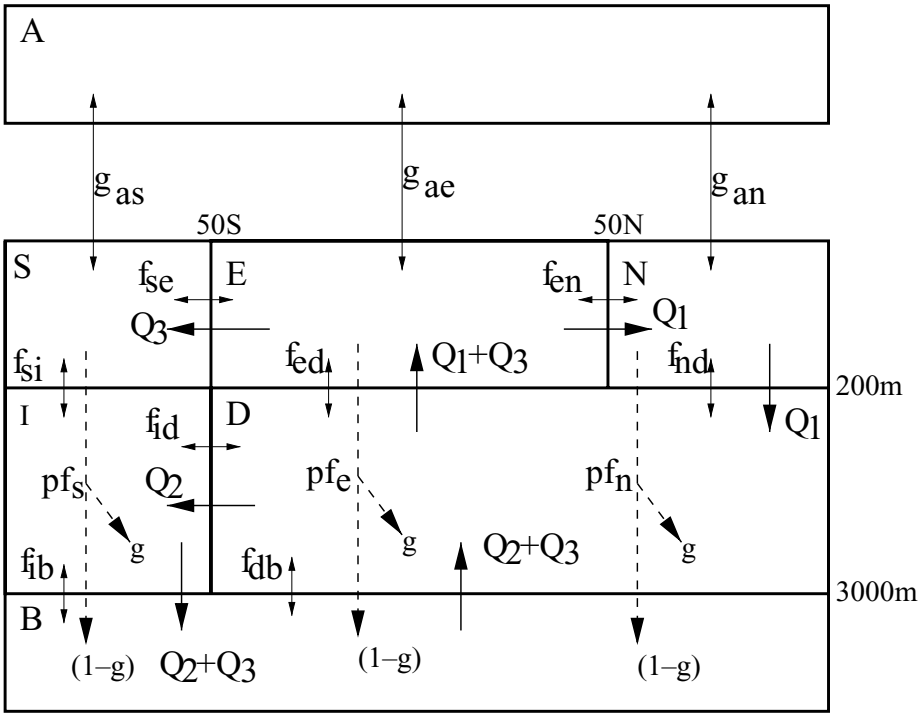

Fig. 1. Diagram of the six-box model (not to scale). Shown are the Atmosphere box (A), the Southern surface box (S), the low-latitude surface or Equatorial box (E), the Northern surface box (N), the deep southern or Intermediate box (I), the Deep box (D) and the Bottom box (B). The density-driven thermohaline flow is shown as Q_1, Q_2, and Q_3. f_{xy} denotes mixing between boxes x and y, g_{ax} is the air–sea gas exchange constant and *pf* is the particulate flux.

Equatorial "E", and Northern oceans "N". The three other boxes are a Deep box "D" (which the Northern box flows into), a deep southern or Intermediate box "I", and a lower or Bottom box "B" (which the southern latitudes flow into). The flows $Q1$ and $Q2 + Q3$ can be thought of as representing North Atlantic Deep Water (NADW) and Antarctic Bottom Water (AABW), respectively.

We have followed Dugdale (1967) with the "extension of the Michaelis and Menten enzyme kinetics to whole organisms" by including an MM-type feedback relating nutrient concentration to export production:

$$p_{\mathrm{f}} = K \times \frac{P}{P + P_{\mathrm{phos}}} \tag{1}$$

where p_{f} is the particulate flux out of a given surface box; P is the phosphate concentration in the surface box; K is the rate constant and P_{phos} is the half-saturation constant. We tune K and P_{phos} to achieve both export production within reasonable ranges (Falkowski et al., 1998) and acceptable phosphate and other nutrient concentrations in the various boxes. The export production depends not only on the phosphate levels but also on other nutrients that are not included in our model such as iron and nitrogen. Because levels of these nutrients vary over the ocean surface, K was tuned separately in each of the surface boxes.

The main differences between this model and most other box models applied to the atmospheric glacial–interglacial CO_2 problem can be summarized as follows: this model has a dynamically consistent flow field (meaning the flow field changes as the density-field changes, rather than being prescribed a priori); the particulate flux follows an MM-type feedback; the magnitude of export production is in good agreement with observations; there are horizontal and vertical mixing terms between all boxes; the E box is allowed to have a non-zero phosphate concentration; and a freshwater flux between boxes is included in the model (Table 2). The effect of including a dynamic flow field and a nutrient feedback is to change model sensitivity to perturbations of various parameters in different regions. A detailed explanation of the model construction and derivation can be found in Appendix A.

3. Model parameters

The parameters and the tracer distributions are tuned to be consistent with the global mean values. Areas were computed from Levitus: the area of ocean north of 50°N is 7% of the total; the area south of 50°S is 13% of the total; the remainder (Equatorial box, 'E') has 80% of the ocean area. These areas are consistent with the volumes of ocean over which mean concentrations were computed.

Mixing coefficients were estimated as follows. The eddy-mixing coefficient for vertical mixing in the interior non-polar

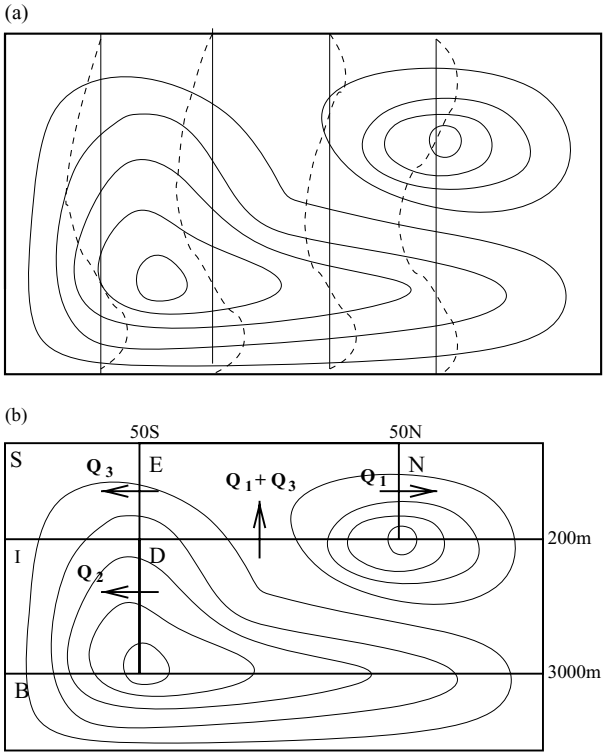

Fig. 2. Diagrams of (a) the stream functions and the shape functions, (b) boxes and fluxes.

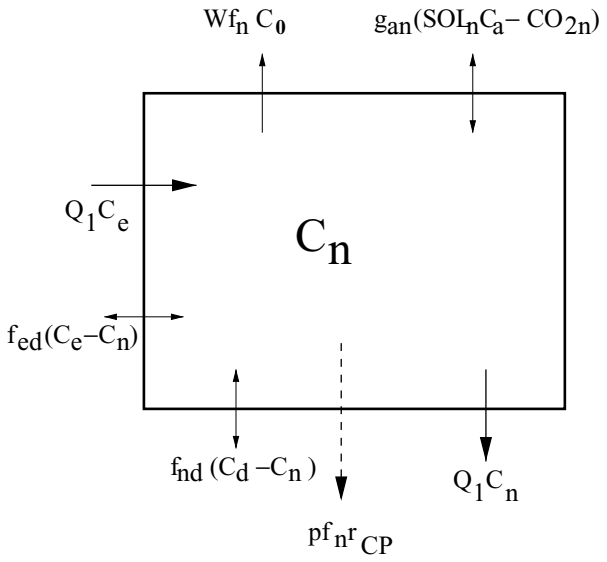

Fig. 3. Fluxes of carbon dioxide into and out of the N box. C_a is the atmospheric pCO_2. CO_{2n} is the dissolved CO_2 in the N box which is a function of ΣCO_2, alkalinity, temperature and salinity.

ocean was required to be between 1×10^{-5} and 1×10^{-4} m^2 s^{-1}, in line with observational evidence (Polzin et al., 1997). In the southern box, where intense mixing along steeply inclined isopycnals yields a large effective vertical mixing coefficient, and in the northern box, where deep convection also yields high effective mixing, an effective vertical eddy-mixing coefficient between 10^{-3} and 10^{-2} m^2 s^{-1} was used. This takes into account eddy-mixing on scales not resolved by the model. It should be noted that while the mixing coefficients prescribed in the polar boxes of the model are roughly 100 times larger than those in the non-polar box (Table 1), the actual exchange fluxes (which depend both on mixing coefficient and box area) in the polar boxes are only a factor of 3–5 larger than in the non-polar box (the non-polar box having a far greater area than the polar boxes). A more recent study of the mixing in the Nordic Seas (Garabato et al., 2004) finds diffusivities ranging from 10^{-4} to 10^{-2} m^2 s^{-1} in the deep (>2000 m) ocean, compared to the cannonical background value of 1×10^{-5} m^2 s^{-1} which was observed in the quieter eastern basins.

The horizontal eddy-mixing coefficient was estimated to be between 2 and 3×10^3 m^2 s^{-1}, in line with values used in GCMs (http://climate.lanl.gov/Models/POP/UsersGuide.pdf). The vertical and horizontal "best-guess" mixing coefficients were then multiplied by the area between adjacent boxes and divided by a mean length-scale in order to get an estimate of the volume flux of water exchanged by two boxes by mixing: $F_{Sv} \approx (K_v \times$ Area)/distance. The length-scales used to compute net horizontal exchange between boxes are given in Table 1. (The large length-scales are necessary to capture the very low-frequency behaviour, and average mixing across very large areas of space.)

We set the air–sea gas exchange constants to be consistent with a piston velocity of 3 m d^{-1}, following Broecker and Peng (1982). The surface boundary condition for salinity and other concentration variables is a fixed flux which represents evaporation or dilution. We specify fresh water fluxes, Wf_n, Wf_s, from the non-polar box to the polar boxes. This flux represents the net evaporation over precipitation and runoff in the non-polar region and transfer of this water to the polar regions (total amount of water is conserved). Thus, the surface flux depends on a reference value of each quantity (C_0 in the case of $\Sigma\ CO_2$) multiplied by this fresh water flux.

Nutrients are transferred from the surface boxes to the deeper boxes through particulate fluxes, pf_s, pf_e, pf_n. A fraction, g, of the particulate flux is dissolved in the deep (I and D) boxes with the remainder dissolving in the bottom (B) box (see Fig. 1). There is no sedimentary reservoir included in our box model, so all particulate matter leaving the surface boxes is remineralized at depth. Based on the results of Milliman and Troy (1999) and Sarmiento et al. (2002), we assume an export ratio of $CaCO_3$ to organic carbon of 0.1. This is significantly lower than the value of around 0.2 used by previous carbon-cycle box-model studies (Toggweiler, 1999; Archer and Winguth, 2000), and also by Peacock et al. (2006).

From (A7), it can be seen that λ, which sets the absolute magnitude of the flows, is also a tunable parameter. This was adjusted to give the Northern flow rate (Q_1) to be around 15 Sv in order to reflect the present magnitude of the NADW (Schmitz, 1995). Table 4 gives the flow rates obtained based on these requirements.

Table 1. Estimated mixing coefficients, effective fluxes, areas and length-scales used in the interglacial solution

Mixing terms	Eddy-mixing coefficient ($m^2\ s^{-1}$)	Estimated flux (Sv)	Area (m^2)	Length scale (m)
Vertical				
f_{si}	2.6×10^{-3}	80	4.68×10^{13}	1500
f_{ib}	2.4×10^{-3}	60	4.68×10^{13}	1900
f_{ed}	6.5×10^{-5}	12.5	2.88×10^{14}	1500
f_{db}	6.1×10^{-5}	10	3.13×10^{14}	1900
f_{nd}	2.2×10^{-3}	37.5	2.52×10^{13}	1500
Horizontal				
f_{se}	2.5×10^{3}	0.3	2×10^{9}	1.7×10^{7}
f_{en}	2.3×10^{3}	0.3	2×10^{9}	1.6×10^{7}
f_{id}	2.5×10^{3}	4	2.8×10^{10}	1.8×10^{7}

The parameters used to obtain the glacial and interglacial solutions (Tables 6 and 7) are given in Tables 2 and 3.

The stoichiometric ratios used in the model were calculated using the revised Redfield ratios of Anderson and Sarmiento (1994) ($r_{\text{Corg:P}} = 117$; $r_{\text{O2:P}} = 170$; $r_{\text{N:P}} = 16$; Table 2). To compute the ratio of total carbon (soft tissue plus carbonate) to phosphate, $r_{\text{C:P}}$, it was assumed that a fraction $(1 - \gamma)$ of the particulate flux is organic matter, and fraction γ is calcium carbonate: $r_{\text{C:P}} = r_{\text{Corg:P}}/(1 - \gamma)$. The ratio $r_{\text{Alk:P}}$ was calculated in a similar manner, using $r_{\text{Alk:P}} = 2\gamma r_{\text{C:P}} - r_{\text{N:P}}$. The soft-tissue contribution is given by $r_{\text{N:P}}$ (negative because degradation of organic matter in the deep ocean decreases alkalinity while increasing dissolved inogranic carbon, DIC). For the carbonate pump, alkalinity is affected twice as much as DIC, and so this contribution is $2\gamma r_{\text{C:P}}$. Note that there is a strong dependence of $r_{\text{Alk:P}}$ on the choice of γ, and on the choice of stoichiometric ratio $r_{\text{Corg:P}}$. In earlier carbon cycle box models, significantly higher values than those used here were chosen for both these parameters, yielding a significantly higher estimate of $r_{\text{Alk:P}}$.

4. Model solutions

The model described in Appendix A was initialized with estimated pre-industrial mean tracer concentrations and run to steady state. An upper-ocean restoring temperature boundary condition was applied with a relaxation time-scale of 30 d; the salinity boundary condition was applied as a net freshwater flux into and out of the ocean (the values used for the glacial and interglacial boundary conditions are given in Table 3). We ran the model in three different modes: The first was with fixed-flow and prescribed particulate flux, which is akin to the traditional box model applied to the glacial–interglacial atmospheric pCO_2 problem (e.g. Sarmiento and Toggweiler, 1984; Siegenthaler and Wenk, 1984; Knox and McElroy, 1984). The model was also run in dynamic-flow mode with fixed particulate flux; and finally in dynamic-flow mode with an MM-type feedback of particulate flux on nutrient concentration included. Fluxes between boxes were prescribed based on present-day climatology in the fixed-flow model; in the dynamic-flow variants of the model, the flow was computed based on the model density structure, as described in Appendix A.

The model interglacial and glacial states are similar to those presented in Peacock et al. (2006). The differences are mainly due to our having adopted different estimates of the stoichiometric ratios (see Table 3) and the rain ratio (following Sarmiento et al., 2002) in this study.

4.1. Interglacial model solution

The restoring ocean–surface temperature boundary condition used to obtain the Interglacial (modern) solution was 0°C for the southern box, 20°C for the non-polar box, and 5°C for the northern box. These values are not the exact average values computed from the Levitus data, but are well within the one standard deviation error bar. The reason for using values slightly lower than the averages in the high-latitude boxes is that this brings the deep-ocean temperature more into line with observations. In the real ocean, deep convection occurs on a very localized scale in cold high-latitude waters. The mean tracer values of the high-latitude boxes in the box model are somewhat different to the tracer properties which are communicated to the deep ocean via the process of deep convection. This is a fundamental shortcoming of box models in general, and one reason why it is quite difficult to match observed deep-ocean properties in such a framework.

The parameters used in obtaining the interglacial solution are given in Tables 2 and 3. Table 6 gives the model tracer concentrations for the interglacial solution. The salinity and oxygen concentrations predicted by the model are, for the most part, within the one standard deviation error bar computed from the data. However, in the bottom box, the model oxygen is slightly lower than one standard deviation from the Levitus average, and in the deep box, the oxygen concentration is significantly lower than the mean (although within the one standard deviation error bar).

Table 2. Parameter values used in both interglacial and glacial models. Note the width has been factored out

Parameter		Interglacial and Glacial
Box volume (10^6 km^3)	Southern	9.36
	Low latitude	57.6
	Northern	5.04
	Southern Deep	131.04
	Deep	876.96
	Bottom	360
Temperature relaxation time (d)		30
Piston velocity (m d^{-1})		3
Fraction of particulate flux remineralizing in D&I boxes	g	0.8
Fraction of $CaCO_3$ in sinking particles	γ	0.1
Redfield ratios	$r_{\mathrm{Corg:P}}$	117
	$r_{\mathrm{C:P}}$	$r_{\mathrm{CorgP}}/(1\text{-}\gamma)$
	r_{O2}: P	170
	$r_{\mathrm{N:P}}$	16
	$r_{\mathrm{Alk:P}}$	$2\gamma\, r_{\mathrm{C:P}} - r_{\mathrm{N:P}}$
Flow parameters (km^2 yr^{-1})	λ_1	35 345
	λ_2	136 080
	λ_3	9720
	λ_4	111 340
	λ_5	7953
Freshwater flux (km^2 yr^{-1})	Wf_{s}	1.3
	Wf_{n}	0.3
Particulate flux		
Rate constant (mol m^{-1} yr^{-1})	K_{s}	3.8×10^4
	K_{e}	5.7×10^5
	K_{n}	1.6×10^5
Half-saturation constant (μmol m^{-3})	P_{phos}	0.05

Table 3. Parameter values used which differed for the glacial and interglacial solutions

Parameter		Interglacial	Glacial
Restoring temperature (°C)	Southern	0	−1.8
	Low latitude	20	16
	Northern	5	1
Initial salinity (‰)		34.7	36.0

Table 4. Flow rates for thermohaline flow in interglacial and glacial solutions

Flow (Sv)	Interglacial	Glacial
Q_1	15.03	11.81
Q_2	10.59	4.98
Q_3	8.66	4.07

Table 5. Particulate flux in each surface box for interglacial and glacial solutions

Particulate flux (g C m^{-2} yr^{-1})	Interglacial	Glacial
Southern	15.49	15.48
Non-polar	24.19	18.52
Northern	109.06	99.42
Total (Gt C yr^{-1})	13.05	10.70

This reveals a fundamental limitation of this model; in order to increase the deep and bottom oxygen, either the vertical mixing must be increased, or the high-latitude export production must be reduced. A significant decrease in export production is required to obtain a relatively modest increase in deep-ocean oxygen concentration, while increasing vertical mixing increases the high-latitude nutrient concentrations to values above those observed. Because the model includes an MM-type feedback on surface nutrient concentration, increasing the nutrient concentration also increases the particulate flux, which leads to higher oxygen consumption in the deep ocean. One possible resolution to this dilemma is to develop a model with higher vertical resolution. It does not seem possible with the current configuration of the model to have a significantly higher deep oxygen concentration and maintain a phosphate concentration in the northern box around 0.5 mmol m^{-3}, which is in line with observational evidence. The approach taken with earlier box-model studies (Knox and McElroy, 1984; Sarmiento and Toggweiler, 1984; Toggweiler, 1999) was to construct a model with just one high-latitude box, and to allow the mean phosphate concentration to be very high (much higher than Northern Hemisphere observations, closer to that in the Southern Hemisphere) in this box. This, combined with high vertical mixing, and a very low particulate flux (an order of magnitude lower than Falkowski et al., 1988 estimates) resulted in oxygen levels in the deep boxes somewhat higher than those reported here, but this is clearly at the expense of approximating reality in other areas.

The phosphate concentrations in this solution are in good agreement with observational evidence. The southern box has a value of around 1.5 mmol m^{-3}, the northern box of close to 0.5 mmol m^{-3}; and the non-polar box of 0.08 mmol m^{-3}. (It should be remembered that the non-polar box extends to 50°N and 50°S.) The surface pCO_2 is in fair agreement with the Takahashi et al. (1999) data. The model's northern high latitudes is a sink of CO_2, while the low latitudes and southern box are a

small source. Also in agreement with present-day observations, the northern ocean is much further out of local equilibrium with the atmospheric pCO_2 than either the low latitude or southern box. The northern downwelling is just over 15 Sv. The southern downwelling is around 9 Sv giving a total surface downwelling of 24 Sv.

The export production in the interglacial solution follows a similar spatial gradient to that of Falkowski et al. (1998), with a total global export production of 13.05 Gt C yr^{-1}. Falkowski et al. (1998) estimated a total net export production for the present day of the order of 16 Gt C yr^{-1}; the box-model value is in fair agreement with the observational estimate, and *much* higher than the export production typical of box models (see Archer and Winguth (2000) for discussion).

4.2. Glacial model solution

In order to obtain a glacial model state, starting at the interglacial solution given above, the following changes were made.

(1) Restoring temperatures were reduced to -1.8° in the Southern box; 16° in the low-latitude box, and to 1° in the Northern box. Mean ocean salinity was increased to 36‰.

(2) The northern mixing term was reduced by 30% and the southern mixing terms by 50%.

(3) The initial condition for alkalinity was increased by 40 meq m^{-3} and the initial condition for ΣCO_2 by 20 mmol m^{-3}. In addition, the initial condition for PO_4 was modified such that there was an increase in mean-ocean phosphate of 0.123 mmol m^{-3} (this is the change expected by attributing roughly a third of the observed benthic δ^{13} C shift to storage in shelf sediments).

The glacial solutions (Table 7) also agree well with existing proxy data. Further details, and justification for making the above changes to obtain a glacial state, can be found in Peacock et al. (2006). In this paper, we limit ourselves to taking two distinct solutions, interglacial and glacial, and considering the sensitivity of these solutions to small perturbations. More specifically, we are concerned with the sensitivity of distinct model solutions to various parametrizations, and how different assumptions in model construction can influence apparent "high-latitude sensitivity." The model solutions for the interglacial (pre-industrial) ocean and the Last Glacial Maximum (glacial) are shown in Tables 6 and 7. These are the solutions on which we perform LSA.

Table 6. Solution for interglacial. Temperature is given in °C, salinity in ‰. The concentrations of PO $_4$, ΣCO_2 and O_2 are given in mmol m^{-3}, pCO_2 is given in ppmv and alkalinity is given in m eq m^{-3}. A, S, E, N, I, D and B correspond to the regions illustrated in Fig. 1

Tracer	A	S	E	N	I	D	B
T	-	0.15	19.95	5.24	2.01	4.70	2.25
S	-	34.55	34.98	34.80	34.62	34.72	34.63
PO_4	-	1.53	0.08	0.50	2.08	2.36	2.49
ΣCO_2	-	2205	2043	2129	2290	2345	2345
pCO_2	277.73	284.94	282.11	230.42	-	-	-
ALK	-	2369	2381	2374	2320	2378	2383
O_2	-	337	239	314	188	60	110

Table 7. Solution for glacial. Key as for Table 6

Tracer	A	S	E	N	I	D	B
T	-	−1.72	15.97	1.22	0.41	2.28	0.74
S	-	35.70	36.38	36.14	35.88	36.03	35.91
PO_4	-	1.48	0.05	0.25	2.24	2.38	2.87
ΣCO_2	-	2195	2045	2119	2322	2363	2407
pCO_2	202.00	208.18	206.47	155.27	-	-	-
ALK	-	2397	2425	2412	2416	2427	2424
O_2	-	350	259	337	130	30	11

5. Previous metrics of high-latitude sensitivity

There are two widely cited metrics of "high-latitude sensitivity" which have been used to illustrate a fundamental difference between box models and GCMs. These are Broecker's "HBEI index" (Broecker et al., 1999) and Archer's "abiotic pCO_2" (Archer and Winguth, 2000). As we will demonstrate, neither the HBEI nor the abiotic pCO_2 indices are ideal or all-encompassing measures of high-latitude sensitivity.

5.1. HBEI

5.1.1. Definitions. The HBEI index as defined for box models (Broecker et al., 1999) provides a measure of how close a particular model solution lies to one of two extreme member states (one dominated by oceanic transport of pCO_2, and the other by atmospheric transport of pCO_2). A low value of the index implies that a perturbation to the physical/chemical properties in the low-latitude ocean will have a minimal impact on atmospheric pCO_2.

However, the HBEI has been defined slightly differently for box models and GCMs (Bacastow, 1996; Broecker et al., 1999) and it is in no way apparent that these definitions are comparable. For box models, the HBEI (BM-HBEI hereafter) is calculated by comparing atmospheric pCO_2 (or alternatively pCO_2 in the low-latitude ocean box) for extreme changes in the air–sea gas exchange rate and oceanic circulation rate (Broecker et al., 1999, eq. 2). The steady-state atmospheric pCO_2 (pCO_2^0) is compared with the atmospheric pCO_2 obtained assuming rapid gas exchange (pCO_2^{gasex}), and that obtained by assuming rapid circulation (pCO_2^{circ}). The BM-HBEI is then calculated as

$$\text{BM-HBEI} = \frac{pCO_2^0 - pCO_2^{\mathrm{gasex}}}{pCO_2^{\mathrm{circ}} - pCO_2^{\mathrm{gasex}}}. \quad (2)$$

Table 8. Mean and standard deviation concentrations of temperature, salinity and oxygen in the different ocean boxes. Values computed from the Levitus annual average data set

Tracer		S	E	N	I	D	B
T	mean	1.69	19.03	5.66	1.35	4.39	1.15
(°C)	s.d.	2.55	6.58	3.28	1.20	3.66	0.72
S	mean	34.13	35.17	33.95	34.64	34.70	34.73
(‰)	s.d.	0.23	0.98	1.16	0.14	0.46	0.08
O_2	mean	311.62	207.30	282.12	209.07	149.08	189.28
(mmol m^{-3})	s.d.	34.60	55.15	49.18	13.21	73.54	37.71

For GCMs, the HBEI (GCM-HBEI hereafter) is estimated by perturbing the solubility coefficient in the low latitudes (between 40°S and 40°N; Broecker et al., 1999, eq. 4). The GCM-HBEI is then calculated as

$$\text{GCM-HBEI} = \frac{\text{pCO}_2^f - \text{pCO}_2^0}{\text{pCO}_2^i - \text{pCO}_2^0}, \tag{3}$$

where pCO_2^0 is the steady-state atmospheric pCO_2; pCO_2^i is the atmospheric pCO_2 obtained using the perturbed solubility coefficient in the non-polar box, but not allowing any readjustment to occur; and pCO_2^f is the steady-state atmospheric pCO_2, obtained after perturbing the solubility in the non-polar regions and letting the model run to a new steady-state.

5.1.2. Application to our model. Using the values given in Broecker et al. (1999), and comparing fast gas-exchange versus fast ocean-circulation scenarios, we obtain a BM-HBEI value of between 0.04 and 0.07 (depending on which steady-state solution is used).

For the interglacial solution:

$$\text{BM-HBEI} = (277.73 - 265.37)/(541.08 - 265.37) = 0.0448.$$

For the glacial solution:

$$\text{BM-HBEI} = (202.00 - 186.92)/(417.38 - 186.92) = 0.0654.$$

By the HBEI-metric, these values would place our model firmly in the strongly "high-latitude sensitive" camp.

However, when we calculate the GCM-HBEI with our model using the solubility-perturbation method, a value of around 0.4 is obtained, which is in line with the GCM-HBEI calculated from GCMs, and is considered to be representative of a model which is *not* particularly high-latitude sensitive.

For the interglacial solution:

$$\text{GCM-HBEI} = (276.94 - 277.73)/(275.78 - 277.73) = 0.4051.$$

For the glacial solution:

$$\text{GCM-HBEI} = (201.33 - 202.00)/(200.55 - 202.00) = 0.4621.$$

Although both definitions of the HBEI measure the same sort of behaviour, and have the same end-members (0 and 1), the scaling between the two end-members for BM-HBEI and GCM-HBEI is different (eqs. 2 and 3). In order to provide a meaningful measure of differences between models, a consistent definition for HBEI needs to be used.

5.2. *Abiotic pCO_2*

Abiotic pCO_2 can be thought of as a measure of a mean ocean temperature with which atmospheric CO_2 equilibrates. Under prescribed initial conditions, a low value of the abiotic pCO_2 index corresponds to a relatively low effective equilibration temperature, which has been taken to imply greater high-latitude sensitivity. Abiotic pCO_2 is defined for an ocean with no active biological pump. As explained in Archer and Winguth (2000), this index is computed for an abiotic ocean by reducing mean ocean Σ CO_2 and alkalinity to compensate for the removal of carbon by the biological pump. It should be noted that the value of abiotic pCO_2 obtained for a given model is not really measuring sensitivity to a perturbation at all; it yields no information whatsoever on the response of a model to changes in parameters.

Following the recipe in Archer and Winguth (2000), our model yields an abiotic pCO_2 of 221 ppmv, in line with previous box models. Abiotic pCO_2 can be increased to 255 ppmv, a value similar to that seen in GCMs, by a tenfold increase in low-latitude mixing. However, this would give unreasonable results in the usual biotic case. The abiotic pCO_2 is the same regardless of whether we are considering the fixed-flow model, or the dynamic model with or without MM feedback, and thus does not give any information on how these features affect the model. As we will see in later sections, these three versions of the model differ considerably, especially in their sensitivity.

6. Linearized sensitivity analysis

LSA is a particularly attractive sensitivity analysis technique due to its general applicability and simple interpretation. Significant progress has been made computationally, making LSA a practical and competitive technique (see Restrepo et al., 1998 for a

strategy and code that circumvents its storage expense; `http://www-unix.mcs.anl.gov/autodiff/ADIFOR/` for automatic differentiation tools; and DASPK v3.0, available at `www.engineering.ucsb.edu/~cse`, for code specifically designed for this type of sensitivity analysis).

LSA can be used to compare the sensitivity of a given model to infinitesimal perturbations in any number of selected parameters. Using this approach, it is very straightforward to consider the impact on a tracer, such as atmospheric pCO_2, of varying a given parameter in a given box. We may simultaneously compare the relative importance of all the parameters on the model outcome. Strictly speaking, the analysis applies only locally. In practice, however, the results may be more widely applicable. Naturally, care must be taken in making global conclusions based on the sensitivity to infinitesimal perturbations of the model about a particular solution. However, this is not an issue in our case, since we are only interested in perturbations about two steady-state solutions, and these can be evaluated fully and separately. We may also use LSA to infer whether parameters or state vector components can be eliminated from the model, based on their minimal impact on the solution.

With LSA, we seek to determine the sensitivity of the model to fixed- and dynamic-flow conditions, and the effect of including a feedback between surface-ocean nutrient concentration and particulate flux. We will also identify the parameters of greatest impact to the model solutions, focusing in particular on empirically adjusted parameters. In the context of our problem, the procedure may be explicitly described as follows. The system of algebraic and differential equations that represents the evolution of the tracers in the boxes can be written as

$$\frac{\partial \mathbf{u}}{\partial t} = \mathbf{F}(\mathbf{u}, \mathbf{p}) \tag{4}$$

where $\mathbf{u}$ is the "state" vector of dimension $\dim(\mathbf{u}) = N$ containing the tracers; $\mathbf{p}$ is the "parameter" vector of dimension $\dim(\mathbf{p}) = M$. The steady-state solution, $\tilde{\mathbf{u}}$, is found by solving

$$\mathbf{F}(\tilde{\mathbf{u}}, \mathbf{p}) = 0. \tag{5}$$

There may be multiple steady-state solutions which may be stable or unstable, but we are assuming that we are interested in a particular, stable, steady-state solution.

The matrix $\frac{\partial \tilde{\mathbf{u}}}{\partial \mathbf{p}}$ yields the sensitivity of the steady-state solution, $\tilde{\mathbf{u}}$, with respect to changes in the parameters, $\mathbf{p}$:

$$\frac{\partial \tilde{\mathbf{u}}}{\partial \mathbf{p}} = -\left[\left.\frac{\partial \mathbf{F}}{\partial \mathbf{u}}\right|_{\mathbf{u}=\tilde{\mathbf{u}}}\right]^{-1} \left.\frac{\partial \mathbf{F}}{\partial \mathbf{p}}\right|_{\mathbf{u}=\tilde{\mathbf{u}}} \tag{6}$$

where $\frac{\partial \mathbf{F}}{\partial \mathbf{u}}$ is the Jacobian matrix of $\mathbf{F}$ with respect to $\mathbf{u}$, and $\frac{\partial \mathbf{F}}{\partial \mathbf{p}}$ is the Jacobian matrix of $\mathbf{F}$ with respect to $\mathbf{p}$, both evaluated at the steady-state vector. The conservation equations for salinity, phosphate, carbon and alkalinity provide constraints that make a reduced $\frac{\partial \mathbf{F}}{\partial \mathbf{u}}$ nonsingular. The dimensions of the sensitivity matrix is $N \times M$.

Excerpts from the sensitivity analysis are shown in Table 9. Results are shown for both the 278-ppmv interglacial solution and the 202-ppmv glacial solution. Because linearized sensitivity only deals with infinitesimal perturbations about a given steady-state solution, these may be different from the actual value obtained given a finite change. Table 9 shows the results for three cases: the model in fixed-flow mode; the model in dynamic-flow mode, and the model in dynamic-flow mode with the addition of the MM-type feedback on nutrient concentrations. Each column in Table 9 shows the sensitivity (for the steady-state solution) of atmospheric pCO_2 to selected parameter changes.

With the exception of temperature, the sensitivity matrix has been normalized so that it gives the percentage change of atmospheric pCO_2 (compared to its average atmospheric value) for a 10% perturbation to the parameter of interest. In the case of temperature (because it is not an extensive variable), we consider a 1°C change. For example, the first column in the first row gives the percentage change in atmospheric pCO_2 due to a 1°C change in the southern box restoring temperature.

7. General comments on the results from LSA

We have considered the results from LSA applied to atmospheric pCO_2 for a number of the model parameters. Inspection of the results of the sensitivity analysis reveals significant differences in the response of each of the models to perturbations, and differences for a given model in the response to perturbations in different parameters. We begin by making a few general comments on the results presented in Table 9.

(1) Previous studies in which "high-latitude sensitivity" was diagnosed made the prescription based on models with just a single high-latitude box (e.g. Sarmiento and Toggweiler, 1984). Our box model differs fundamentally from such box models, and from "Stommel-type" models in that it has distinct high-latitude boxes, and is not symmetrical. We find with our model that the separate high-latitude boxes can exhibit very different behaviour with regard to sensitivity. For example, consider the temperature perturbation to the dynamic-flow model with the MM feedback (the interglacial solution is shown in the upper left-hand panel of Figs. 4 and 5 by the triangles). The southern box exhibits quite a strong response to a 1° temperature perturbation (6 ppmv), while the northern box exhibits a very muted response (0.9 ppmv). The low-latitude box response falls between the two (2.9 ppmv). Thus, we might describe this particular model variant as having "southern high-latitude sensitivity". This is clearly not true for the northern box, which exhibits only a fraction of the sensitivity of the southern box. The asymmetry is an important consideration, as it is clearly a feature of the "real" ocean. In future discussion of whether or not a model is "high-latitude sensitive", it might be prudent to specify which hemisphere one is referring to in the debate.

(2) A model may exhibit sensitivity in one region whose sign is opposite to the sensitivity in another region. For example, if one considers the sensitivity to a perturbation in the air–sea

Table 9. Results of the LSA; results are shown for three-box model versions for both the interglacial and glacial solutions. Shown is the sensitivity of atmospheric pCO_2 to changes in various parameters. The parameters shown are the surface temperature in the southern, low-latitude, and northern boxes, respectively; the vertical mixing; the particulate fluxes; air–sea fluxes; and g; (see Fig. 1 and Table 2 for description of parameters). The sensitivities give the ppmv change in atmospheric pCO_2 for a 10% change in a given parameter (except in the case of temperature, in which case we consider a 1°C change). C_a is the atmospheric pCO_2 sensitivity for various different models, and both glacial and interglacial solutions

	Interglacial C_a^{FIXED}	Glacial C_a^{FIXED}	Interglacial $C_a^{DYNAMIC}$	Glacial $C_a^{DYNAMIC}$	Interglacial $C_a^{DYNAMIC_MM}$	Glacial $C_a^{DYNAMIC_MM}$
T_{atms}	4.69	3.48	2.43	0.69	6.00	5.01
T_{atme}	3.71	2.97	12.33	12.08	2.89	1.92
T_{atmn}	2.84	2.59	2.92	4.08	0.90	0.50
f_{si}	3.59	3.11	3.90	3.59	3.25	2.62
f_{ed}	3.40	3.66	4.31	4.94	0.07	−0.16
f_{nd}	3.55	2.76	3.56	2.43	2.76	1.41
Kpf_s	-	-	-	-	−1.09	−1.22
Kpf_e	-	-	-	-	−1.60	−0.47
Kpf_n	-	-	-	-	−2.54	−1.51
g_{as}	0.23	0.17	0.23	0.17	0.23	0.17
g_{ae}	0.12	0.15	0.12	0.15	0.12	0.15
g_{an}	−1.18	−1.33	−1.18	−1.33	−1.18	−1.33
g	1.54	2.23	1.54	2.23	0.05	0.59

gas exchange coefficient (Fig. 5), atmospheric pCO_2 changes in a positive sense (increase) if there is a perturbation increasing air–sea gas exchange in the Southern Hemisphere, whereas atmospheric pCO_2 decreases if the same perturbation is applied to the northern box. Thus, it becomes important to distinguish not only between which region is most sensitive to a given perturbation, but also how the sign of the response changes regionally (i.e. negative or positive sensitivity).

(3) Details of model construction (e.g. specifying a fixed versus a dynamic flow field) can *completely* change the results of the sensitivity analysis. For example, in the case where the mixing coefficient was perturbed by 10% (right-hand panels of Fig. 4), for both the glacial and interglacial solutions, the model exhibits the classic high-latitude sensitivity for the dynamic-flow model which incorporates the MM-type feedback (triangles), but shows the opposite effect (low-latitude sensitivity) for the dynamic-flow model which does not include the MM-type feedback (circles). The difference is especially striking in the sensitivity analysis applied to the glacial solution (lower right-hand panel of Fig. 4). Thus, even slight changes to the parametrizations in a single model can have a profound effect on apparent model sensitivity.

(4) The solution about which sensitivity is calculated (for a specified model configuration) can also have a large impact on the results obtained by such an analysis. An example of this is given by the mixing coefficient perturbation (Fig. 4, Table 3). In the fixed-flow model (squares), the interglacial solution gives a result which exhibits weak high-latitude sensitivity, whereas the glacial solution gives a result which is slightly low-latitude sensitive.

(5) The results also depend on relative to what the model sensitivity is measured. For example, if one considers the response of the dynamic-flow model without the MM feedback (circles in Fig. 4) to a temperature perturbation, the model would be labelled strongly "low-latitude sensitive" (left-hand panels in Fig. 4). By contrast, if one considers the response to a perturbation of the air–sea gas exchange coefficient (Fig. 5), the model appears to have a near-zero response to a perturbation to the low latitudes, but a much more pronounced response to a perturbation in the northern box.

(6) Although we have only shown the response of atmospheric pCO_2 to perturbations in various parameters, one might also need to consider the response of, for example, deep-ocean oxygen concentration to a response in various parameters. This is a natural part of LSA; indeed, the formalism outlined in Section 6 yields the sensitivity of *all* tracers to all parameters.

8. Response of atmospheric pCO_2 to a temperature perturbation

While analysis of the full sensitivity matrix (this being the sensitivity of every tracer in the model to a specified change in every model parameter) lies beyond the scope of this paper, an understanding of what controls the differences in the sensitivity of

Table 10. Variables and parameters used in the box model equations; subscripts 's', 'e', 'n', 'd', 'b' and 'a' indicate the box. Subscript 0 means a reference concentration. Note the width has been factored out

T_α	Temperature in box α (°C).
S_α	Salinity in box α (‰).
P_α	Phosphate in box α (mol m^{-3}).
C_α	Total carbon dioxide in box α (mol m^{-3}).
A_α	Alkalinity in box α (eq m^{-3}).
O_α	Oxygen in box α (mol m^{-3}).
V_α	Area of box α (depth × length) (m^2).
$T_{\text{atm}\alpha}$	Restoring temperature for box α (°C).
τ	Relaxation time (yr).
$\kappa_\alpha = \frac{V_\alpha}{\tau}$	Relaxation time-scale for box α (m^2 yr^{-1}).
SOL $_\alpha$	Solubility of CO_2 in box α (mol m^{-3} atm^{-1}).
Wf_α	Fresh water flux into box α (m^2 yr^{-1}).
$f_{\alpha\beta}$	Mixing between boxes α and β (m^2 yr^{-1}).
$g_{a\beta}$	Air–sea gas exchange constant (m^2 yr^{-1}).
Q_n	Water flow (m^2 yr^{-1}).
pf_α	Particulate flux from box α (mol m^{-1} yr^{-1}).
K_α	Rate constant (mol m^{-1} yr^{-1}).
$P_{\text{phos}\alpha}$	Half-saturation constant (mol m^{-3}).
g	Fraction of particulate flux that remineralizes in the D box.
r_{XP}	Redfield ratio of X with respect to phosphate (mol X/mol P).
C_a	Partial pressure of carbon dioxide in atmosphere (atm).
$CO_{2\alpha}$	Dissolved carbon dioxide in box α (mol m^{-3}).

each of the three models (fixed, dynamic and dynamic MM) can be gleaned by considering the response of atmospheric pCO_2 to a temperature perturbation in various regions.

There are several ways by which temperature may affect atmospheric pCO_2. The final sensitivity of a particular model configuration depends on both choice of model configuration, and on the relative strengths of various parameters.

The most obvious way by which temperature can have an effect on atmospheric pCO_2 is via solubility. An increase in restoring temperature causes a decrease in solubility of CO_2 in the region in question. ΣCO_2 decreases due to outgassing of CO_2 which in turn increases atmospheric pCO_2. Depending on where the perturbation occurs, and the details of model circulation, the temperature perturbation or the locally depressed ΣCO_2 (or locally elevated pCO_2) may be transmitted to other surface boxes. These factors in turn affect atmospheric pCO_2.

In the dynamic-flow models, temperature perturbations have an additional effect through perturbation of the density gradient, and hence the flow field. If the temperature perturbation is such that the fluxes are reduced, this tends to lower the net input of ΣCO_2 into the surface boxes (Σ CO_2 being much higher in the deep ocean). At constant temperature (i.e. for the boxes which do not have a temperature perturbation applied), this will cause a slight decrease in pCO_2 which decreases atmospheric pCO_2. Conversely, a temperature perturbation that increases fluxes may cause an increase in atmospheric pCO_2.

The effect of including an MM-type feedback in a model depends on the relative magnitude of the prescribed particulate flux in the corresponding model without an MM feedback. If the MM feedback reduces the particulate flux in a given region over that in the model without MM feedback, nutrients in that model region will be slightly higher than in the non-MM model, and both ΣCO_2 and pCO_2 will tend to increase slightly (less nutrient drawdown). In general, the MM feedback is a negative one. Models which include the MM feedback tendto have a somewhat muted sensitivity relative to dynamic-flow models without this feedback. This effect is most apparent in the non-polar box, as the relationship between phosphate and particulate flux in the MM formalism becomes steeper for lower phosphate concentrations.

We now consider temperature perturbations to the three surface boxes, and explain how the different models will respond to provide the observed atmospheric pCO_2 change.

8.1. Perturbation to the southern box

An increase in the southern box restoring temperature causes a decrease in ΣCO_2 and an increase in pCO_2 in the southern box through reduced solubility. This drives up the atmospheric pCO_2 by the air–sea gas exchange. Because the temperature perturbation is only applied to the southern box, the temperature (and hence solubility) does not change notably in the non-polar and northern boxes. Thus, the pCO_2 in these boxes increases (due to atmospheric transport), and drives up the ΣCO_2. The net effect in the fixed-flow model is an increase in atmospheric pCO_2 of 4.7 ppmv for the interglacial solution and 3.5 ppmv for the glacial solution (Table 9).

In the dynamic-flow model, a temperature increase in the southern box restoring temperature also decreases the overturning fluxes (Q_1, Q_2 and Q_3). In the dynamic model without the MM feedback, this change cannot alter the particulate flux. Therefore, the only impact on atmospheric pCO_2 is through changes to the surface ΣCO_2 and alkalinity, which are caused by changes in the flow field. The reduced fluxes in the dynamic-flow model result in slightly less high-ΣCO_2 water upwelling from the deep ocean into the non-polar box and hence slightly lower ΣCO_2 and pCO_2 in the non-polar box over the fixed-flow model. This lower-ΣCO_2, lower-pCO_2 signal, propagates to the northern and southern boxes through the surface fluxes, resulting in a somewhat muted response of atmospheric pCO_2 to the temperature perturbation relative to the fixed-flow model.

The difference between the dynamic-flow model which includes the MM feedback and the one which does not is in the magnitude of the particulate flux. In this case, incorporation of the MM-feedback results in a particulate flux out of the non-polar box which is lower in the model with the MM feedback. This results in higher nutrient levels in the non-polar box relative to the fixed-particulate-flux case, which leads to higher ΣCO_2,

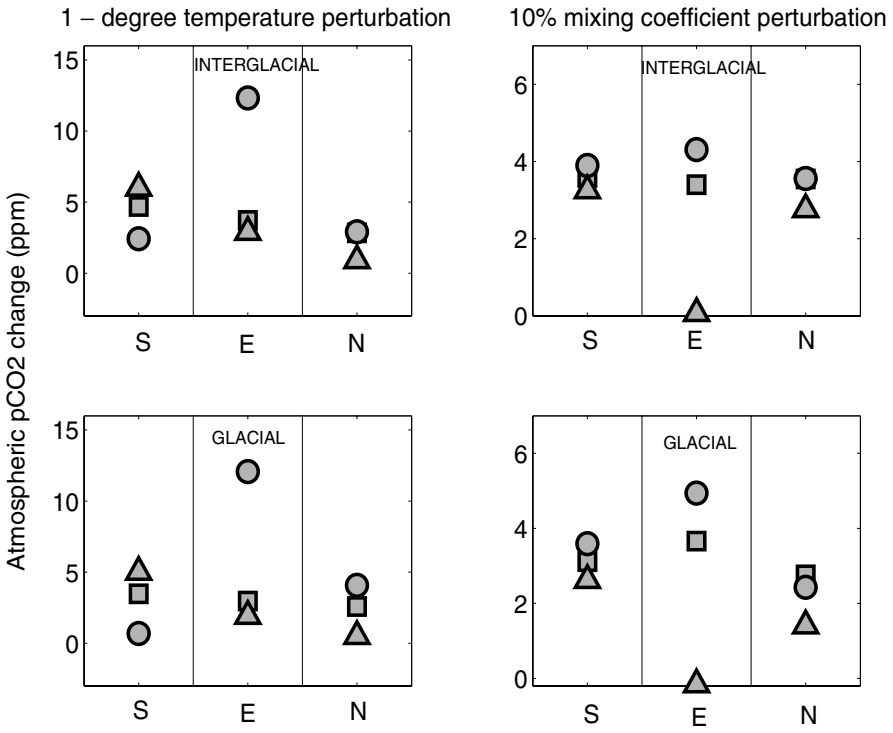

Fig. 4. Results from the LSA (see also Table 9). The left-hand panels show response of atmospheric pCO_2 to a 1°C temperature perturbation in each of the model surface boxes (northern N, low-latitude E, and southern S); the right-hand panels show the response to a 10% perturbation in the vertical mixing coefficient. The upper panels show sensitivity analysis about interglacial solutions and lower panels show analysis about glacial solutions. The squares show the results from the fixed-flow model; the circles show the results from the dynamic-flow model with no MM feedback; the triangles show results from the dynamic-flow model which includes the MM feedback.

and at constant temperature, higher pCO_2. The particulate fluxes out of the northern and southern boxes due to the southern box temperature perturbation are actually relatively unchanged. It is only at the limit of low phosphate concentration that MM feedback has a strong effect. The net impact on atmospheric pCO_2 in the dynamic model with the MM feedback is slightly larger than thatin the other two models; a 1°C S-box temperature increase causes an increase in atmospheric pCO_2 of 6 ppmv for the interglacial solution, and 5 ppmv for the glacial solution (Table 9).

8.2. Perturbation to the equatorial box

Under fixed-flow conditions, the solubility effect of a 1°C temperature increase in the restoring temperature over the non-polar (equatorial) box is to cause an increase in atmospheric pCO_2 of 3–3.7 ppmv. As expected, the higher restoring temperature boundary condition over the non-polar box causes outgassing of CO_2. Thus, ΣCO_2 decreases and pCO_2 increases in the non-polar box. Changes to the ΣCO_2 and pCO_2 in the high-latitude boxes are determined by two competing processes: atmospheric and oceanic transport. The circulation acts to decrease the ΣCO_2 of the high-latitude boxes, while the atmospheric transport acts to increase the pCO_2 and thus ΣCO_2 in the polar boxes. The net result in the fixed-flow model is a slight increase in atmospheric pCO_2 for a positive temperature perturbation to the non-polar box.

Under dynamic-flow conditions, an increase in the non-polar box restoring temperature not only affects the solubility in the non-polar box, but also increases the horizontal density gradients. Thus, the overturning circulation is enhanced and the phosphate and ΣCO_2 in the non-polar box increase. In the dynamic-flow model without the MM feedback, the ΣCO_2 in the non-polar box is significantly higher than thatin the fixed-flow case. The ΣCO_2 and pCO_2 in the northern and southern boxes increase via Q_1 and Q_3, causing a far stronger response in atmospheric pCO_2 than thatin the fixed-flow case. In this prescribed particulate flux model, the response of atmospheric pCO_2 to a 1°C temperature increase in the non-polar box is very large: an increase of over 12 ppmv for both the interglacial and glacial solutions.

This large response is significantly moderated by incorporation of the MM feedback. In the case of the dynamic-flow model *with* the MM feedback, the response of atmospheric pCO_2 to

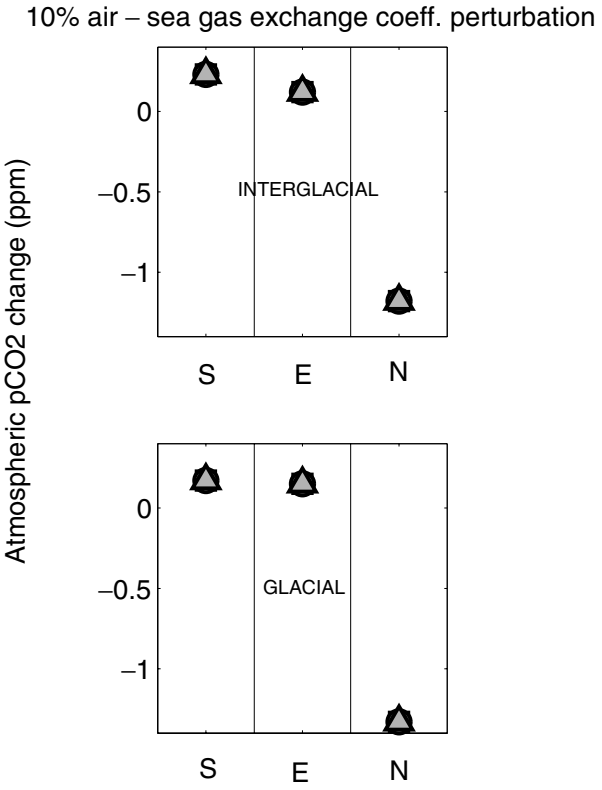

Fig. 5. Results from the LSA (see also Table 9). This figure shows the response to a 10% perturbation in the air–sea gas exchange constant (northern N, low-latitude E, and southern S). Labels as for Fig. 4.

the same 1°C temperature perturbation is only an increase of 2.9 ppmv for the interglacial, and 1.9 ppmv for the glacial solution.

This large difference in response can be explained as follows. In the dynamic-flow model without MM, there is significantly increased upwelling but the particulate flux is unaffected. Overall surface ΣCO_2 and pCO_2 are increased dramatically. The inclusion of the MM feedback, however, triggers a higher particulate flux out of the non-polar box, and hence a larger drawdown of nutrients and ΣCO_2. This leads to a reduction in pCO_2 in the non-polar box in the model. This low-pCO_2 signature (compared to that in the dynamic-flow model without the MM feedback) is advected to the polar boxes and, subsequently, the increase in atmospheric pCO_2 is far less pronounced in the model which includes the MM feedback than the increase in atmospheric pCO_2 in the model with fixed particulate flux.

8.3. Perturbation to the northern box

Increasing the restoring temperature boundary condition in the northern box, under fixed-flow conditions, leads to a decrease in the ΣCO_2 and an increase in pCO_2 in the northern box. This increases atmospheric pCO_2, which feeds back to increase the pCO_2 in the southern and non-polar boxes. Because the northern box downwells directly into the deep box, there is no oceanic circulation effect equivalent to that seen in the non-polar box temperature perturbation case. The net effect of the northern box temperature perturbation for the fixed-flow model is an increase in atmospheric pCO_2 of 2.6–2.8 ppmv for the solutions considered here.

In the dynamic-flow cases, in addition to the solubility effect, the other major effect of increasing the temperature in the northern box restoring boundary condition is to raise the temperatures in the northern and deep boxes. This has the effect of decreasing the density gradient between the non-polar and northern boxes while increasing the density gradient between the deep and intermediate boxes. This decreases Q_1 and increases both Q_2 and Q_3. This latter change has a large impact on the southern box. Since the mixing term f_{si} remains unchanged while Q_3 increases, this causes a relative depletion of ΣCO_2 in the southern box over the fixed-flow case. pCO_2 in the southern box decreases because the temperature in this box is relatively unchanged. This counteracts the increase in northern box pCO_2. The net effect is a relatively modest impact on atmospheric pCO_2 of the northern box temperature perturbation.

The difference between the dynamic-flow model with the MM feedback and that with the fixed particulate flux comes in the slightly elevated particulate flux, and hence increased drawdown of nutrients and ΣCO_2 in the model with the MM feedback. This further mutes the response of the atmospheric pCO_2 to the northern box temperature perturbation by the same mechanism described for the non-polar box.

9. Discussion

It is evident from the different sensitivities reported in Table 9 and from the discussion in Sections 7 and 8, that the solution about which sensitivity is computed, the parameter to which one is measuring sensitivity, and the incorporation of a dynamic flow field or the addition of an MM-type particulate flux dynamics, can all introduce feedbacks which significantly affect model sensitivity.

Frequently, high-latitude sensitivity has been taken to mean the sensitivity of atmospheric pCO_2 to a change in temperature (e.g. Bacastow, 1996; Archer and Winguth, 2000). By this measure, none of the three model variants we considered appears to exhibit high-latitude sensitivity (Fig. 4). For the interglacial solutions, the dynamic-flow model without MM actually exhibits a sensitivity of atmospheric pCO_2 to a temperature perturbation of the non-polar box that is about four times higher than the sensitivity of either high-latitude box. Both the fixed-flow model and the dynamic-flow model with MM show a greater sensitivity to a southern-box temperature perturbation than to a northern-box temperature perturbation, with the non-polar-box sensitivity lying between that of the two high-latitude boxes (Fig. 4).

The sensitivities of various regions in a given model to changes in the air–sea gas exchange coefficient are of interest, especially in light of some recent hypotheses put forward to explain part of the glacial–interglacial pCO_2 drawdown. It has been widely suggested that the growth of sea-ice might be responsible for increasing stratification of the high-latitude ocean (e.g. Stephens and Keeling, 2000). If this were the case, it might also be expected that there would be a corresponding decrease in the rate of air–sea gas exchange in the polar oceans. Lowered air–sea gas exchange over the Glacial Southern Ocean has been suggested by Francois et al. (1997) and Stephens and Keeling (2000), among others, as a possible means by which to regulate atmospheric pCO_2 on glacial–interglacial time-scale. We find that reduction in the Southern Ocean air–sea gas exchange constant g_{as} of 10% leads only to a minimal (fraction of 1 ppmv) drawdown of atmospheric pCO_2. It is clear from this example and from the LSA results (Table 9), that for the box model developed here, the effect of reducing air–sea gas exchange constant on atmospheric pCO_2 is very small. [This is in line with the findings of Archer et al. (2003), who cut off gas exchange polewards of 55°S, and found a significant pCO_2 drawdown only in two of the six models they tested.]

As discussed in Section 7 and clearly seen in Figs. 4 and 5, it is not only details of model parametrizations which can have a profound effect on apparent sensitivity. Different hemispheres can exhibit very different sensitivities to a given parameter change, necessitating the distinction between "northern high-latitude sensitivity" and "southern high-latitude sensitivity" in certain cases. For example, while there is almost no response to perturbations of the air–sea gas exchange constant in the non-polar box, the northern box shows a much stronger and oppositely signed sensitivity than the southern box (Fig. 5 and Table 9).

It should also be noted from Fig. 5 and Table 9 that the sensitivity is the same for the air–sea gas exchange for all three models. This is because there are no feedbacks associated with this parameter in the model. The air–sea gas exchange affects neither the temperature or salinity (which would in turn affect the flow through density gradients), nor its phosphate levels where the MM dynamics would come into play.

The relative response of a given tracer in a given region to a perturbation not only depends on model configuration and parametrizations, but it can (and does) alsochange significantly depending on the steady-state solution about which the LSA is performed. This is most clearly seen in the perturbation of the mixing coefficient in the fixed-flow model (squares in Fig. 4), where the interglacial solution exhibits weak high-latitude sensitivity, while the glacial solution exhibits weak low-latitude sensitivity.

When the model is run in fixed-flow mode, it is not possible to achieve a feedback between particulate flux, circulation and atmospheric pCO_2. However, in the dynamic-flow model, this feedback can be quite important, particularly in the non-polar box. Closely related to this, it is not possible in fixed-flow mode to affect non-temperature-dependent surface properties (such as phosphate) via temperature perturbations. The only way to change phosphate via a temperature perturbation (and hence the particulate flux via MM) is to change the flow field. In general, of the three model variants considered here, it is the dynamic-flow model *without* the MM feedback which displays the strongest sensitivity to perturbations.

In dynamic-flow models, even a small change in the density field triggers a change in circulation, which feeds back on the atmospheric CO_2. For example, a slight reduction in equator–pole temperature gradient feeds back to decrease equatorial upwelling. This decreases the supply of nutrient-rich, high-ΣCO_2 deep water to the surface ocean. At constant temperature, this implies a decrease in pCO_2 in the surface ocean. If, in addition, an MM-type feedback is included, reduced nutrient levels can cause the particulate flux to fall, moderating the effect on atmospheric pCO_2.

The response of atmospheric pCO_2 to a temperature perturbation is different in terms of bothmagnitude and spatial gradient not only between the fixed-flow and dynamic-flow modes for a given solution, but also between dynamic models with and without the MM-type feedback, and between the different steady-state solutions. In neither the glacial nor interglacial solutions, and in neither the fixed- nor the dynamic-flow modes, is there evidence of the strong "high-latitude sensitivity" observed in previous box models (Archer and Winguth, 2000; Archer et al., 2003). These results are more in accord with those of Bacastow (1996), who found that ocean GCMs did *not* display the extreme high-latitude sensitivity of atmospheric pCO_2 to a temperature perturbation characteristic of fixed-flow, prescribed particulate-flux box models.

In the simple model, we have presented here, the equator–pole temperature gradient can be decreased *either* by lowering the restoring temperature boundary condition in the non-polar box, *or* by increasing the high-latitude restoring temperature. In the absence of circulation changes, a decrease in the restoring temperature acts to pull down atmospheric pCO_2, while an increase acts to raise atmospheric pCO_2. Addition of a dynamic-flow field can amplify or reduce the effect that changing the temperature restoring boundary condition has on the fixed-flow model (as discussed in Section 8). Inclusion of an MM feedback on particulate flux may partly mitigate the effects of the dynamic flow with fixed particulate flux. Thus, the different effects compete to provide the overall effect.

Not only is LSA significantly more useful in its ability to gauge the sensitivity of models (at the same time preserving the essence of the coupling between the different parameters and variables) than are previous metrics of "high-latitude sensitivity", but it also yields results that significantly diminish the generality of assertions that box models are more high-latitude sensitive than

GCMs (see Archer and Winguth, 2000). A good example of this is the sensitivity of the dynamic-flow model without the MM feedback to a temperature perturbation versus a perturbation in the air–sea gas exchange constant. In the case of the perturbation to the air–sea gas exchange constant, the model is more sensitive to high-latitude perturbations (although northern and southern high latitudes differ in the sense of the sensitivity). However, in the case of the temperature perturbation, this model appears "low-latitude sensitive".

Another important distinction is that between the sensitivity of a variable to a specified change in a parameter (such as reported in Table 9), and the absolute change to be expected in a parameter between glacial and interglacial conditions. To the linear approximation, this will be the sensitivity (as reported in Table 9) multiplied by the absolute change in that parameter. This will give a measure which might be quite different for each box than is the sensitivity to a percent (or degree) change in a given parameter. The problem with considering "absolute sensitivity" is that, for many parameters, the actual magnitude of the glacial–interglacial change in that parameter is poorly (if at all) known. For example, we have little idea how the air–sea gas exchange rate changed between glacial and interglacial times. It might be argued that, due to stronger winds, it was somewhat higher during glacial times, but alternately, increased ice cover may have meant that it was lower. The absolute magnitude of the change, and how this change varied with latitude, is open to speculation. For the purposes of model comparison, the absolute change is fairly irrelevant; one should first seek to determine whether or not two different classes of models exhibit similar or different patterns of sensitivity to perturbations in specified parameters.

10. Conclusions

We have developed a box model for long time-scale, zonally averaged, low-dimensional oceanic flow and chemistry. This model has been shown to be consistent with the lowest-order approximation of the thermohaline equations, but is also endowed with characteristics present in the higher-order and non-linear equations. We have demonstrated in a separate paper (Peacock et al., 2006) that this box model was able to reproduce many of the chemical and physical characteristics of the glacial and interglacial oceans.

In gauging the sensitivity of the model solutions to changes in parameters and state variables, we employed LSA. In addition to being highly efficient and generally applicable, the method takes into account the complex couplings within a model. LSA is far more of an all-encompassing metric than previous measures of "high-latitude sensitivity"; not only is it easily applied to the ocean carbon-cycle questions considered in this work, but it could also be used to study features such as model sensitivity to discretization errors (a potentially important consideration when one is forced to use low resolution to capture flows at large spatio-temporal scales, typical of oceanic climate simulations).

The adoption of a more rigorous and robust method to gauge the sensitivity of model goes a long way towards reducing the debate over fundamental differences in various model genres. Application of LSA to the model developed herein has been used to demonstrate that significant differences in sensitivity exist between the following:

(1) Models with fixed and dynamic flow fields.
(2) Models with a dynamic-flow model which includes an MM-type feedback and those with prescribed export production.
(3) Different steady states of the same model.
(4) Different regions within a model (e.g. northern versus southern high-latitude oceans).
(5) Perturbations to different parameters in a given model.

Claims about the sensitivity of atmospheric pCO_2 drawdown to changes in various parameters from earlier box-type models which have a fixed-flow field and/or fixed particulate flux should be interpreted with caution. This is especially true for metrics such as the HBEI, which have different definitions for different classes of model. In light of the many factors which can influence model sensitivity listed above, the debate over comparisons between box models and GCMs will need to be re-evaluated. Before possible box-model-based mechanisms for the drawdown of atmospheric pCO_2 in glacial times are rejected or accepted, it will be necessary to use a more comprehensive and rigorous tool (such as LSA) for comparing the sensitivity of various classes of model than has hitherto been used.

Looking to the future, it is likely that with increasing atmospheric pCO_2, there will undoubtedly be changes in parameters such as sea-surface temperature, as well as in mean winds, which will affect parameters such as air–sea gas exchange constant and the rate of upper-ocean mixing. It is important to have some idea of how spatial uptake of CO_2 by the ocean might change in the future due to changes in multiple parameters. For example, a temperature perturbation might cause a strong drawdown of atmospheric pCO_2 in the low-latitude oceans, but a change in wind strength might cause a far stronger response in the high-latitude oceans. In seeking an understanding of the possible trajectories of future climate change, it will be necessary to distinguish between the relative importance of such changes in regulating atmospheric pCO_2.

11. Acknowledgments

This work, LA-UR 02-7081, was carried out in part at Los Alamos National Laboratory under the auspices of the Department of Energy and supported by contract W-7405-ENG-36. We also received support from NSF/ITR, Grant DMS-0113649

(JMR). We wish to thank the Center for Nonlinear Studies at Los Alamos for their hospitality and financial support (EL). Thanks also to two anonymous referees, whose comments proved very useful in improving the presentation and content of this paper.

12. Appendix A: Derivation of the tracer equations

As was recognized by Cessi and Young (1992), the thermohaline asymptotic equations obtained under the scaling assumptions they used have certain topological symmetries that are not entirely realistic. In particular, the lowest-order thermohaline equations fail to capture crucial aspects evident in simulations of the fully parametric global circulation at the appropriate time- and length-scales. Rather than using asymptotic machinery, we use an unconventional approach to capturing the important higher order effects of the thermohaline circulation. We circumvent the lowest-order flow symmetries by using kinematic arguments on the flow and the vertical eigenfunctions defining the flow.

The setting is an effectively two-dimensional shallow ocean, idealized as a rectangular basin of ℓ extent in the latitudinal y-direction, and depth d, in the z-direction. The basin is impermeable on all sides except for the upper boundary, which is exposed to the atmosphere. The idealized equations for the zonally averaged thermohaline motion of an incompressible fluid are

$$\frac{\partial \mathbf{v}}{\partial t} = -\mathbf{v}\cdot\boldsymbol{\nabla}\mathbf{v} - \frac{1}{\rho_0}\boldsymbol{\nabla}\Pi + \nu\boldsymbol{\nabla}^2\mathbf{v} - \hat{\mathbf{z}}g(\rho/\rho_0), \tag{A1}$$

$$\boldsymbol{\nabla}\cdot\mathbf{v} = 0. \tag{A2}$$

Here $\mathbf{v}\,(y, z, t) = (v, w)$ is the velocity field, which can also be written in terms of the stream function Ψ via the relation $\mathbf{v} = (-\partial_z\Psi, \partial_y\Psi)$. Π is the pressure, ρ_0 is the average value of the density ρ, $\hat{\mathbf{z}}$ is the vertical unit vector, and ν the fluid viscosity. The buoyancy of the fluid is related to $T(y, z, t)$ and $S(y, z, t)$ (the temperature and salinity of the fluid) through the linearized equation of state

$$-g(\rho/\rho_0) = g(\alpha_{\mathrm{T}}T - \alpha_{\mathrm{S}}S),$$

where g is gravity, and α_{T} and $-\alpha_{\mathrm{S}}$ are the thermal and saline expansion coefficients, respectively. For presentation purposes, the equation of state is assumed to be linear here, but in application of the model we adopt the fully non-linear expression.

All tracers and chemical species are assumed to be passive and to obey an equation of the form

$$\frac{\partial\Theta}{\partial t} + \mathbf{v}\cdot\boldsymbol{\nabla}\Theta = \kappa_\Theta\boldsymbol{\nabla}^2\Theta + J(\Theta), \tag{A3}$$

where Θ is the tracer, κ_Θ is the eddy diffusivity and $J(\Theta)$ is a source or sink term.

The equations are non-dimensionalized as follows: $(y, z) \to d\,(y/\epsilon, z)$, $t \to d^2t/\kappa_{\mathrm{T}}\,\epsilon^2$, $\Psi \to \kappa_{\mathrm{T}}/\epsilon\Psi$, $T \to \nu\kappa_{\mathrm{T}}/(g\alpha_t d^3\,\epsilon^2)\,T$, $S \to \nu\kappa_{\mathrm{T}}/(g\alpha_{\mathrm{S}}d^3\epsilon^2 S)$. The Prandtl number is $\sigma \equiv \nu/\kappa_{\mathrm{T}}$, $L \equiv \kappa_{\mathrm{S}}/\kappa_{\mathrm{T}}$ is the Lewis number, and $\epsilon \equiv d/\ell$ the aspect ratio.

Boundary conditions on the stream function are free-slip on all sides of the domain. At the air–sea interface, we impose the scaled temperature $T = a(y)$, and the salt flux $S_z = b(y)$, where $a(y) \equiv \Delta T(y)\,g\,\alpha_{\mathrm{T}}\,d^3\,\epsilon^2/(\nu\,\kappa_{\mathrm{T}})$ and $b(y) \equiv \Delta S(y)\,g\,\alpha_{\mathrm{S}}\,d^3\,\epsilon^2/(\nu\,\kappa_{\mathrm{T}})$. We assume that the other boundaries are insulated in temperature and salinity. The boundary conditions on the other tracers will be detailed below. Following Cessi and Young (1992), we assume that

$$\begin{aligned}(\Psi, T, S) &= \epsilon(\Psi_1, T_1, S_1) + \epsilon^2(\Psi_2, T_2, S_2) + \ldots,\\ a &= \epsilon a_1 + \epsilon^2 a_2 + \ldots,\\ b &= \epsilon^3 b_3 + \epsilon^4 b_4 + \ldots,\end{aligned} \tag{A4}$$

and consider the distinguished limit $\epsilon \to 0$. The full development of the asymptotic expansion and its analysis appears in Cessi and Young (1992) and Thual and McWilliams (1992).

In the development of the model, we invoke the following assumptions or *conditions*.

(1) Conservation of the tracers salinity, carbon (including the atmospheric box), phosphate and alkalinity (note that temperature and oxygen may have a surface flux, so are not strictly conservative).

(2) Conservation of mass via incompressibility, an assumption in the Boussinesq approximation.

(3) Conservation of momentum.

(4) The structure of the flow depicted in Fig. 2a (deep sinking in both high-latitude regions, with deep water formed in the Southern Ocean underriding that from the North Atlantic) is captured.

(5) The flow is assumed to be stably density stratified, over the long time-scales of glaciation. Hence, the density must be the same throughout every column or increase monotonically with increasing depth.

(6) The velocity and its first derivative are assumed continuous for all time. Shearing by opposing flows is not permitted.

The flow we seek to capture [condition (4)] is depicted schematically in Fig. 2a (note the vertical dimension is not drawn to scale). Water sinks in both polar regions, with that sinking in the Southern Hemisphere being denser and hence underriding the water sinking in the Northern Hemisphere. This flow is considered one appropriate for the study of glacial–interglacial oceanic dynamics for a number of reasons. There are numerous data which show that the two regions in the ocean in which water sinks to the deep ocean to drive a thermohaline circulation are around the Antarctic perimeter in the Southern

Hemisphere, and in the far North Atlantic. The dense southern water is found in the lowermost kilometre of the ocean throughout the South Atlantic, Pacific and Indian Oceans, and evidence for its distinct tracer characteristics have been noted for over a century. GCMs also capture this 'two-cell' thermohaline circulation, as is depicted in the zonally averaged stream function in Fig. 2.

The number and topology of the boxes in our model are chosen to capture the above flow. Six boxes was the minimum number to achieve our desired goals. We assume that these regions are not time-dependent and that they have a very simple geometry. The model is relatively robust to the details of the geometry. Relative sizes of boxes are important but the exact positions of their boundaries are not. Once these regions are determined we develop simple ordinary differential equations for the box-averaged dynamic quantities. This averaging procedure eliminates small-scale phenomena which, for some tracers, cannot be ignored. In these cases, the phenomena are added to the appropriate tracer equations in parametric form, that is, in the form of mixing coefficients, particulate flux and the like.

The lowest-order temperature equation in the asymptotic analysis on (A1), (A2) and (A3) yields $T_1 = a_1(y)$. The typical shape of $a(y)$ (and for that matter, the shape of the salt flux) is such that three zones can be distinguished in this forcing: a "non-polar", and two high-latitude "polar" oceanic zones. This suggests that near the surface of the ocean it is possible to minimally define three boxes: the Southern (S), Equatorial (E), and Northern (N) boxes. We set the depth of these boxes as 200 m, although the thermocline is deeper than this; other biological processes of interest are shallower. This value is chosen as a balance between the two requirements. It is also in line with past values. We assume that the E box spans from 50°S to 50°N. Condition (6) on the velocity (mentioned above) implies that if there is upwelling or downwelling in the E box, it is due to both of the circulations. Whether upwelling or downwelling occurs in the E box is strongly dependent on both the salt flux and the temperature at the surface. In the thermally driven regime, the flow will have an upwelling current in the E box.

The lowest-order momentum equation, obtained by substituting (A4) into (A1) and (A2) yields

$$\frac{\partial^3}{\partial z^3}\frac{\partial \Psi_1}{\partial z} = -\frac{\partial (T_1 - S_1)}{\partial y}, \tag{A5}$$

hence, the lowest-order transverse component of the velocity develops due to transverse variations of the density. This means that density differences between the E and N boxes, the S and E boxes and the I and D boxes, are important in driving the circulations. A full solution of the lowest-order transverse velocity is of the form $Z(z)\frac{\partial (T_1 - S_1)}{\partial y}$, where $Z(z)$ is a cubic polynomial in z. Zeros of this polynomial reflect velocity reversals. Conditions (3), (6), and symmetry considerations (i.e. the fact that Z depends on z alone and is the same throughout the domain) suggest, however, that if the shape function is aligned with the flow reversal of either of the circulations, the other circulation flow reversal cannot be captured. Hence, $Z(z)$ is not an adequate approximation of the shape function depicted in Fig. 2a. Rather than solving for the actual shape function, we will pursue the rest of the construction of the minimal model utilizing what we know about the topology of the flow, using the above flow constraints for guidance.

The lowest-order velocity can be solved for explicitly. The main limitation of the solution in capturing the flow in Fig. 2a has to do with the lack of z dependence in the density, to lowest order. Hence, rather than pursuing higher orders in the velocity equations, we instead pursue restoring depth dependence on the density via the reduced tracer equations for salt and temperature. First, we continue with the definition of the boxes.

We place a stagnation point at each of the circulation centres. The 200-m line in the neighbourhood of the northern circulation is needed to obtain the flow reversal depicted in the figure, consistent with the shape function. The line is continued all the way to latitude 50°S, the end of the E box domain. A line delineating the boundary between the S box and E box must pass through the stagnation point of the southern circulation to obtain the lowest-order transverse velocity as a result of horizontally arranged boxes. This line need not continue to the bottom of the domain. Below the stagnation-point depth, the density is approximately uniform and the velocity does not have flow reversals. However, a flow reversal in the southern circulation is present above its stagnation point depth, which is approximately 3000 m below the surface, so we can draw a horizontal line and thus obtain a B box and a D box. It is noted that conditions (2)–(6), along with (A5) imply that a stagnation point requires at least three vertices emanating from it, and these be arranged either as a regular "T" or an upside down "T".

At this stage, we have presented the nearly complete box model, which is shown in Fig. 2b. To summarize, we have three upper boxes and two lower boxes D and B. At this point the boxes marked S and I are not differentiated. Hence, five boxes are minimally needed to capture the two circulations. Any number of subboxes may be added to this minimal configuration.

Possible differences in the density between the southern region and D box can generate a flow due to density differences. Hence, the southern circulation is composed of two different flows, which we label Q_2 and Q_3. Although not required, we divide the upper southern region into an S box and an I box. This division of the southern region into S and I creates a point with four vertices. The reason this is not a stagnation point is that it cannot be reduced to a minimal vertical three-vertex point. This sixth box is not required to capture the fluid flow. However, it was found to be needed to better resolve tracer differences in the southernmost oceanic region. A sixth box also makes it easier for the model to achieve a stable density stratification over a wider range of parameter space.

Anticipating that the fluxes derived from the box model will require tuning to match the model to three-dimensional timescales and flow rates, it is not necessary to know explicitly what the shape function for the flow is. All that is required is to find the correct dependence of the flow on the density of the boxes. We begin with the northern circulation: Q_1 is then the integral

$$\begin{aligned} Q_1 &= \int_{\text{south}} v\,\mathrm{d}z \\ &= -\int_0^{200} \left.\frac{\partial \Psi}{\partial z}\right|_{50^\circ\mathrm{N}} \mathrm{d}z \\ &= -\Psi(50^\circ\mathrm{N}, 200) + \Psi(50^\circ\mathrm{N}, 0) \\ &= -\Psi(50^\circ\mathrm{N}, 200), \end{aligned} \tag{A6}$$

having used the air–sea interface boundary condition on the stream function. The velocity is integrated along the 50°S. The stream function is zero at the ocean surface, and at the ocean bottom. At the stagnation point the velocity is zero. Note that Q_1 is also equal to $\int_{\text{bottom}} w\mathrm{d}y$, and that these two definitions are equivalent. This is due to incompressibility. To find v, we use (A5), hence to within a scaling parameter λ

$$Q_1 = \lambda[\rho(T_\mathrm{n}, S_\mathrm{n}) - \rho(T_\mathrm{e}, S_\mathrm{e})]. \tag{A7}$$

In the case of flows Q_2 and Q_3, we proceed in similar fashion. The flux Q_3, passing from E box to S box, is defined in terms of the transverse velocity flowing south across the E–S interface. The flux Q_2, passing from D box to I box, is defined in terms of the transverse velocity flowing south across the I–D interface. Finally, in box B, the total flux is $Q_2 + Q_3$ and is associated with the velocity flowing north across an interface that connects the stagnation point to the bottom of the ocean. These conditions imply that both the fluxes Q_2 and Q_3 are proportional to weighted averages of the density differences between boxes E and S, and D and I.

Tracers are assumed to be passive. Their distribution at low frequencies is approximated by well-mixed regions and thus their interbox dynamics are primarily determined by advective effects. The equations for the tracers (ΣCO_2 C, temperature T, salinity S, phosphate P, alkalinity A and oxygen O) appear in Appendix B. The pCO_2 of the atmosphere is tracked to ensure that ΣCO_2 is conserved. Salinity, phosphate and alkalinity are also conserved. Surface oxygen is restored towards its saturated level; likewise surface temperature is restored towards a specified level. Phosphate, ΣCO_2, alkalinity and oxygen are also affected by the flux of particulate matter from the surface to the deep ocean. $CaCO_3$ is factored into the particulate flux (as discussed in the next section), although the small amount of $CaCO_3$ that is buried, rather than remineralized, is not explicitly modelled.

The lowest-order asymptotic equations for the tracers lead to trivial motions. Higher order effects need to be captured and this section describes how these are derived. The development of the box equations will be presented for just one tracer, represented by Θ. The presentation is further limited to one of the surface boxes (N), as the development of the equations for the surface boxes is more general than that for the boxes at depth.

The boundary condition at the air–sea interface for the tracers takes the form of a flux-forcing term (which can be zero), plus the specification of the derivative and/or the value of the tracer at the interface. For example, the fluxes into and out of this particular box for the total carbon dioxide are illustrated in Fig. 3, in dimensional form.

In Fig. 3, $Wf_\mathrm{n}\, C_0$ fixes the z-derivative of the carbon C in box N (representing dilution due to fresh water flux), and $g_{\mathrm{an}}(\mathrm{SOL_n}\, pCO_{2a} - CO_{2n})$ is the forcing flux (giving air–sea gas exchange rate).

For the box-averaged tracer Θ_n, defined as

$$\Theta_\mathrm{n} \equiv \frac{1}{V_\mathrm{n}} \int_{V_\mathrm{n}} \Theta\, \mathrm{d}V,$$

the evolution equation in the N box is

$$\frac{1}{V_\mathrm{n}} \int_{V_\mathrm{n}} \frac{\partial \Theta}{\partial t}\, \mathrm{d}V = \frac{1}{V_\mathrm{n}} \int_{V_\mathrm{n}} \left[\kappa_\Theta \boldsymbol{\nabla} \cdot (1, \epsilon^2) \boldsymbol{\nabla}\Theta - \mathbf{v} \cdot \boldsymbol{\nabla}\Theta + J(\Theta)\right] \mathrm{d}V.$$

Using Gauss' theorem, the integral over the interior of the box is equal to the integral of the fluxes through the four sides of the box. Assuming that Θ is a sufficiently smooth function, the derivative can be taken outside the integral on the left-hand side, obtaining

$$\begin{aligned} V_\mathrm{n} \frac{\partial \Theta_\mathrm{n}}{\partial t} = &\int_{\text{right}} \left[\kappa_\Theta \frac{\partial \Theta}{\partial y} - \Theta v + J(\Theta)\right] \mathrm{d}z \\ &+ \int_{\text{left}} \left[\kappa_\Theta \frac{\partial \Theta}{\partial y} - \Theta v + J(\Theta)\right] \mathrm{d}z \\ &+ \int_{\text{bottom}} \left[\kappa_\Theta \frac{\partial \Theta}{\partial z} - \Theta w + J(\Theta)\right] \mathrm{d}y \\ &+ \int_{\text{top}} \left[\kappa_\Theta \frac{\partial \Theta}{\partial z} - \Theta w + J(\Theta)\right] \mathrm{d}y. \end{aligned} \tag{A8}$$

The four integrals on the right-hand side represent the fluxes through the right-hand, left-hand, bottom and top sides of the box, respectively. Each of these integrals can be calculated separately.

On the top of the box, we use a "rigid-lid" assumption (already implicit in the velocity field derived above). The boundary condition for tracers typified by temperature is

$$\tilde{\kappa}_\mathrm{T} \frac{\partial T}{\partial z} = \tilde{a}(T_{\text{atm}} - T)(y),$$

evaluated at the interface; for tracers typified by the salt, the boundary condition is

$$\tilde{\kappa}_\mathrm{S} \frac{\partial S}{\partial z} = \tilde{b} S_0 E(y),$$

evaluated at the interface. Here, $\tilde{a}$, and $\tilde{b}$ are constants of dimensions of length divided by time, S_0 is a proportionality constant, and $E(y)$ is a dimensionless function describing the balances of

evaporation, precipitation and run-off. The forcing flux determines J_Θ, defined as

$$J_\Theta \equiv \int_{\text{top}} J(\Theta)\,\mathrm{d}y,$$

on the N box.

Changes through the left side of the N box are due to advection into the N box and horizontal mixing, *viz*.,

$$\int_{\text{left}} \left[\kappa_\Theta \frac{\partial \Theta}{\partial y} - \Theta v\right] \mathrm{d}z = Q_1\Theta_\mathrm{e} + f_{\mathrm{en}}(\Theta_\mathrm{e} - \Theta_\mathrm{n}). \tag{A9}$$

Changes through the bottom of the box are

$$\int_{\text{bottom}} \left[\kappa_\Theta \frac{\partial \Theta}{\partial z} - \Theta w\right] \mathrm{d}y = -Q_1\Theta_\mathrm{n} + \tilde{f}_{\mathrm{nd}}(\Theta_\mathrm{d} - \Theta_\mathrm{n}) - \tilde{pf}. \tag{A10}$$

In this case $Q_1 = \int_{\text{bottom}} w\,\mathrm{d}y$. The first term represents pure advection out of the N box; the two other terms represent vertical mixing and particulate flux out of the box. These latter terms may or may not be relevant to a particular tracer. For example, these two terms are absent in the temperature and salinity equations. The right-hand side of the box is the edge of the ocean and we assume there are no fluxes into or out of this boundary. Bringing together eqs. (A8)–(A10), gives an equation for the volume-averaged tracer Θ_n in the N box. For example, the equation for the volume-averaged total carbon dioxide in the N box in dimensional form is given by

$$\begin{aligned}\frac{\mathrm{d}C_\mathrm{n}}{\mathrm{d}t} = \frac{1}{V_\mathrm{n}}(&-Wf_\mathrm{n}C_0 + g_{\mathrm{an}}(\mathrm{SOL_n}C_\mathrm{a} - \mathrm{pCO}_{2n})\\ &+ f_{\mathrm{nd}}(C_\mathrm{d} - C_\mathrm{n}) + f_{\mathrm{en}}(C_\mathrm{e} - C_\mathrm{n})\\ &+ Q_1(C_\mathrm{e} - C_\mathrm{n}) - pf_\mathrm{n}r_{\mathrm{CP}}).\end{aligned}$$

where Wf_n is the freshwater flux into the northern box, and C_0 is the reference level for carbon. There is prescribed mixing between the different boxes. Mixing parameters are denoted by f_{xy}, with the subscripts x and y indicating which two boxes the mixing is between. The air–sea gas exchange constants are similarly denoted by g_{as}, g_{ae}, and g_{an}. The air–sea gas exchange constant is calculated from a piston velocity of 3 m d^{-1} multiplied by the surface area of the box.

13. Appendix B: Equations for the six-box model

The equations for the total carbon dioxide are given in (B1). The concentration of $\Sigma\mathrm{CO}_2$ is tracked in each ocean box and the CO_2 partial pressure (pCO_2) is tracked in the atmospheric box (denoted by C_a). C_α denotes the concentration of $\Sigma\mathrm{CO}_2$ in box α. The flow rates Q_1, Q_2 and Q_3 are taken to be positive. Slightly different equations are required in the case where the flows are reversed. Table 10 lists the variables and parameters used in the six-box model equations. The equations are

$$\begin{aligned}\frac{\mathrm{d}C_\mathrm{s}}{\mathrm{d}t} &= \frac{1}{V_\mathrm{s}}(-Wf_\mathrm{s}C_0 + g_{\mathrm{as}}(\mathrm{SOL_s}C_\mathrm{a} - \mathrm{CO}_{2s})\\ &\quad + f_{\mathrm{si}}(C_i - C_\mathrm{s})\\ &\quad + (f_{\mathrm{se}} + Q_3)(C_\mathrm{e} - C_\mathrm{s}) - pf_\mathrm{s}r_{\mathrm{CP}})\\ \frac{\mathrm{d}C_\mathrm{e}}{\mathrm{d}t} &= \frac{1}{V_\mathrm{e}}((Wf_\mathrm{s} + Wf_\mathrm{n})C_0\\ &\quad + g_{\mathrm{ae}}(\mathrm{SOL_e}C_\mathrm{a} - \mathrm{CO}_{2e})\\ &\quad + f_{\mathrm{se}}(C_\mathrm{s} - C_\mathrm{e}) + f_{\mathrm{en}}(C_\mathrm{n} - C_\mathrm{e})\\ &\quad + (Q_1 + Q_3 + f_{\mathrm{ed}})(C_\mathrm{d} - C_\mathrm{e}) - pf_\mathrm{e}r_{\mathrm{CP}})\\ \frac{\mathrm{d}C_\mathrm{n}}{\mathrm{d}t} &= \frac{1}{V_\mathrm{n}}(-Wf_\mathrm{n}C_0 + g_{\mathrm{an}}(\mathrm{SOL_n}C_\mathrm{a} - \mathrm{CO}_{2n})\\ &\quad + f_{\mathrm{nd}}(C_\mathrm{d} - C_\mathrm{n})\\ &\quad + (f_{\mathrm{en}} + Q_1)(C_\mathrm{e} - C_\mathrm{n}) - pf_\mathrm{n}r_{\mathrm{CP}})\\ \frac{\mathrm{d}C_i}{\mathrm{d}t} &= \frac{1}{V_i}((f_{\mathrm{id}} + Q_2)(C_\mathrm{d} - C_i) + f_{ib}(C_\mathrm{b} - C_i)\\ &\quad + (Q_3 + f_{\mathrm{si}})(C_\mathrm{s} - C_i) + gpf_\mathrm{n}r_{\mathrm{CP}})\\ \frac{\mathrm{d}C_\mathrm{d}}{\mathrm{d}t} &= \frac{1}{V_\mathrm{d}}((Q_1 + f_{\mathrm{nd}})(C_\mathrm{n} - C_\mathrm{d}) + f_{\mathrm{ed}}(C_\mathrm{e} - C_\mathrm{d})\\ &\quad + f_{\mathrm{id}}(C_i - C_\mathrm{d}) + (f_{\mathrm{db}} + Q_2 + Q_3)(C_\mathrm{b} - C_\mathrm{d})\\ &\quad + (pf_\mathrm{e} + pf_\mathrm{n})gr_{\mathrm{CP}})\\ \frac{\mathrm{d}C_\mathrm{b}}{\mathrm{d}t} &= \frac{1}{V_\mathrm{b}}((Q_2 + Q_3 + f_{ib})(C_i - C_\mathrm{b})\\ &\quad + f_{\mathrm{db}}(C_\mathrm{d} - C_\mathrm{b})\\ &\quad + (pf_\mathrm{s} + pf_\mathrm{e} + pf_\mathrm{n})(1 - g)r_{\mathrm{CP}})\\ \frac{\mathrm{d}C_\mathrm{a}}{\mathrm{d}t} &= \frac{1}{V_\mathrm{a}}(g_{\mathrm{as}}(\mathrm{CO}_{2s} - \mathrm{SOL_s}C_\mathrm{a})\\ &\quad + g_{\mathrm{ae}}(\mathrm{CO}_{2e} - \mathrm{SOL_e}C_\mathrm{a})\\ &\quad + g_{\mathrm{an}}(\mathrm{CO}_{2n} - \mathrm{SOL_n}C_\mathrm{a}))\end{aligned} \tag{B1}$$

where V_α is the volume of box α (in the case of the atmosphere, it is the number of moles of gas in the atmosphere divided by the width of the ocean boxes), and $g_{a\alpha}$ is the air–sea gas exchange constant between box α and the atmosphere. SOL_α is the solubility of CO_2 in box α, and is taken to be linearly related to the temperature of the box. $\mathrm{CO}_{2\alpha}$ is the concentration of dissolved carbon dioxide in box α, which is a function of $\Sigma\mathrm{CO}_2$, alkalinity, temperature and salinity. The particulate flux is defined in terms of MM dynamics as

$$pf_x = \frac{K_x P_x}{P_x + P_{\mathrm{phos}}}.$$

Flows Q_1, Q_2 and Q_3 are given by

$$\begin{aligned}Q_1 &= \lambda_1(\rho_\mathrm{n} - \rho_\mathrm{e})\\ Q_2 &= \lambda_2(\rho_i - \rho_\mathrm{d}) + \lambda_3(\rho_\mathrm{s} - \rho_\mathrm{e})\\ Q_3 &= \lambda_4(\rho_i - \rho_\mathrm{d}) + \lambda_5(\rho_\mathrm{s} - \rho_\mathrm{e}),\end{aligned} \tag{B2}$$

where the density ρ is a function of temperature and salinity.

The other tracer equations are as follows:
Temperature

$$\begin{aligned}
\frac{dT_s}{dt} &= \frac{1}{V_s}(\kappa_s(T_{atms} - T_s) + f_{si}(T_i - T_s) \\
&\quad + (f_{se} + Q_3)(T_e - T_s)) \\
\frac{dT_e}{dt} &= \frac{1}{V_e}(\kappa_e(T_{atme} - T_e) \\
&\quad + (Q_1 + Q_3 + f_{ed})(T_d - T_e) \\
&\quad + f_{se}(T_s - T_e) + f_{en}(T_n - T_e)) \\
\frac{dT_n}{dt} &= \frac{1}{V_n}(\kappa_n(T_{atmn} - T_n) + f_{nd}(T_d - T_n) \\
&\quad + (f_{en} + Q_1)(T_e - T_n)) \\
\frac{dT_i}{dt} &= \frac{1}{V_i}((f_{id} + Q_2)(T_d - T_i) \\
&\quad + (Q_3 + f_{si})(T_s - T_i) \\
&\quad + f_{ib}(T_b - T_i)) \\
\frac{dT_d}{dt} &= \frac{1}{V_d}((Q_1 + f_{nd})(T_n - T_d) + f_{ed}(T_e - T_d) \\
&\quad + f_{id}(T_i - T_d) + (f_{db} + Q_2 + Q_3)(T_b - T_d)) \\
\frac{dT_b}{dt} &= \frac{1}{V_b}((Q_2 + Q_3 + f_{ib})(T_i - T_b) \\
&\quad + f_{db}(T_d - T_b)).
\end{aligned} \tag{B3}$$

Salinity

$$\begin{aligned}
\frac{dS_s}{dt} &= \frac{1}{V_s}(-Wf_sS_0 + f_{si}(S_i - S_s) \\
&\quad + (f_{se} + Q_3)(S_e - S_s)) \\
\frac{dS_e}{dt} &= \frac{1}{V_e}((Wf_s + Wf_n)S_0 \\
&\quad + (Q_1 + Q_3 + f_{ed})(S_d - S_e) \\
&\quad + f_{se}(S_s - S_e) + f_{en}(S_n - S_e)) \\
\frac{dS_n}{dt} &= \frac{1}{V_n}(-Wf_nS_0 + f_{nd}(S_d - S_n) \\
&\quad + (f_{en} + Q_1)(S_e - S_n)) \\
\frac{dS_i}{dt} &= \frac{1}{V_i}((f_{id} + Q_2)(S_d - S_i) + f_{ib}(S_b - S_i) \\
&\quad + (Q_3 + f_{si})(S_s - S_i)) \\
\frac{dS_d}{dt} &= \frac{1}{V_d}((Q_1 + f_{nd})(S_n - S_d) + f_{ed}(S_e - S_d) \\
&\quad + f_{id}(S_i - S_d) + (f_{db} + Q_2 + Q_3)(S_b - S_d)) \\
\frac{dS_b}{dt} &= \frac{1}{V_b}((Q_2 + Q_3 + f_{ib})(S_i - S_b) \\
&\quad + f_{db}(S_d - S_b))
\end{aligned} \tag{B4}$$

Phosphate

$$\begin{aligned}
\frac{dP_s}{dt} &= \frac{1}{V_s}(-Wf_sP_0 + f_{si}(P_i - P_s) \\
&\quad + (f_{se} + Q_3)(P_e - P_s) - pf_s) \\
\frac{dP_e}{dt} &= \frac{1}{V_e}((Wf_s + Wf_n)P_0 + f_{se}(P_s - P_e) \\
&\quad + f_{en}(P_n - P_e) \\
&\quad + (Q_1 + Q_3 + f_{ed})(P_d - P_e) - pf_e) \\
\frac{dP_n}{dt} &= \frac{1}{V_n}(-Wf_nP_0 + f_{nd}(P_d - P_n) \\
&\quad + (f_{en} + Q_1)(P_e - P_n) - pf_n) \\
\frac{dP_i}{dt} &= \frac{1}{V_i}((f_{id} + Q_2)(P_d - P_i) + f_{ib}(P_b - P_i) \\
&\quad + (Q_3 + f_{si})(P_s - P_i) + gpf_s) \\
\frac{dP_d}{dt} &= \frac{1}{V_d}((Q_1 + f_{nd})(P_n - P_d) + f_{ed}(P_e - P_d) \\
&\quad + f_{id}(P_i - P_d) \\
&\quad + (f_{db} + Q_2 + Q_3)(P_b - P_d) + (pf_e + pf_n)g) \\
\frac{dP_b}{dt} &= \frac{1}{V_b}((Q_2 + Q_3 + f_{ib})(P_i - P_b) \\
&\quad + f_{db}(P_d - P_b) \\
&\quad + (pf_s + pf_e + pf_n)(1 - g)).
\end{aligned} \tag{B5}$$

Alkalinity

$$\begin{aligned}
\frac{dA_s}{dt} &= \frac{1}{V_s}(-Wf_sA_0 + f_{si}(A_i - A_s) \\
&\quad + (f_{se} + Q_3)(A_e - A_s) - pf_sr_{AP}) \\
\frac{dA_e}{dt} &= \frac{1}{V_e}((Wf_s + Wf_n)A_0 + f_{se}(A_s - A_e) \\
&\quad + f_{en}(A_n - A_e) \\
&\quad + (Q_1 + Q_3 + f_{ed})(A_d - A_e) - pf_er_{AP}) \\
\frac{dA_n}{dt} &= \frac{1}{V_n}(-Wf_nA_0 + f_{nd}(A_d - A_n) \\
&\quad + (f_{en} + Q_1)(A_e - A_n) - pf_nr_{AP}) \\
\frac{dA_i}{dt} &= \frac{1}{V_i}(Q_2(A_d - A_i) + f_{ib}(A_b - A_i) \\
&\quad + f_{id}(A_d - A_i) + (Q_3 + f_{si})(A_s - A_i) \\
&\quad + gpf_sr_{AP}) \\
\frac{dA_d}{dt} &= \frac{1}{V_d}((Q_1 + f_{nd})(A_n - A_d) + f_{ed}(A_e - A_d) \\
&\quad + f_{id}(A_i - A_d) \\
&\quad + (f_{db} + Q_2 + Q_3)(A_b - A_d) + (pf_e + pf_n)gr_{AP}) \\
\frac{dA_b}{dt} &= \frac{1}{V_b}(f_{db}(A_d - A_b) + (Q_2 + Q_3 + f_{ib})(A_i - A_b) \\
&\quad + (pf_s + pf_e + pf_n)(1 - g)r_{AP}).
\end{aligned} \tag{B6}$$

Oxygen

$$\begin{aligned}
\frac{dO_s}{dt} &= \frac{1}{V_s}(-Wf_sO_0 + g_{as}(O_{sats} - O_s) + f_{si}(O_i - O_s) \\
&\quad + (f_{se} + Q_3)(O_e - O_s) + pf_s r_{OP}) \\
\frac{dO_e}{dt} &= \frac{1}{V_e}((Wf_s + Wf_n)O_0 + g_{ae}(O_{sate} - O_e) \\
&\quad + f_{se}(O_s - O_e) + (Q_1 + Q_3 + f_{ed})(O_d - O_e) \\
&\quad + f_{en}(O_n - O_e) + pf_e r_{OP}) \\
\frac{dO_n}{dt} &= \frac{1}{V_n}(-Wf_nO_0 + g_{an}(O_{satn} - O_n) \\
&\quad + f_{nd}(O_d - O_n) \\
&\quad + (f_{en} + Q_1)(O_e - O_n) + pf_n r_{OP}) \\
\frac{dO_i}{dt} &= \frac{1}{V_i}((f_{id} + Q_2)(O_d - O_i) + f_{ib}(O_b - O_i) \\
&\quad + (Q_3 + f_{si})(O_s - O_i) - gpf_s r_{OP}) \\
\frac{dO_d}{dt} &= \frac{1}{V_d}((Q_1 + f_{nd})(O_n - O_d) + f_{ed}(O_e - O_d) + \\
&\quad + f_{id}(O_i - O_d) \\
&\quad + (f_{db} + Q_2 + Q_3)(O_b - O_d) - (pf_e + pf_n)gr_{OP}) \\
\frac{dO_b}{dt} &= \frac{1}{V_b}((Q_2 + Q_3 + f_{ib})(O_i - O_b) \\
&\quad - (pf_s + pf_e + pf_n)(1 - g)r_{OP} \\
&\quad + f_{db}(O_d - O_b)).
\end{aligned} \tag{B7}$$

The solubility of CO_2 in water (SOL_α) and the saturation concentration of oxygen in water ($O_{sat\alpha}$) are both assumed to be linear functions of temperature.

$$\begin{aligned}
SOL_\alpha &= \text{Solubility } CO_2(T_\alpha) \\
&= 60.2 - 1.29T_\alpha \text{ mol m}^{-3} \text{ atm}^{-1}
\end{aligned} \tag{B8}$$

$$\begin{aligned}
O_{sat\alpha} &= \text{Saturated } O_2(T_\alpha) \\
&= 0.345 - 0.0054T_\alpha \text{ mol m}^{-3}.
\end{aligned} \tag{B9}$$

The dissolved CO_2 of the surface boxes is a non-linear function of ΣCO_2, alkalinity, temperature and salinity. The flows Q_i are weighted averages of the horizontal density differences as shown in (B2).

References

Adkins, J. F., McIntyre, K. and Schrag, D. P. 2002. The salinity, temperature, and $\delta^{18}O$ of the glacial deep ocean. *Science* **298**, 1769–1773.

Anderson, L. and Sarmiento, J. 1994. Redfield ratios of remineralization determined by data analysis. *Global Biogeochemical Cycles* **8**, 65–80.

Archer, D., Martin, P., Brovkin, V., Plattner, G.-K. and Ashendel, C. 2003. Model sensitivity in the effect of Antarctic sea ice and stratification on atmospheric pCO_2. *Paleoceanography* **18**(1), 1012.

Archer, D. E. and Winguth, A. 2000. What caused the glacial/interglacial atmospheric pCO_2 cycles? *Reviews of Geophysics* **38**(2), 159–189.

Bacastow, R. B. 1996. The effect of temperature change of the warm surface waters of the oceans on atmospheric CO_2. *Global Biogeochemical Cycles* **10**(2), 319–334.

Beck, J. W., Edwards, R. L., Ito, E., Taylor, F. W., Recy, J., Rougerie, F., Joannot, P. and Henin, C. 1992. Sea-surface temperature from coral skeletal strontium calcium ratios. *Science* **257**(5070), 644–647.

Broecker, W. and Peng, T.-H. 1982. *Tracers in the Sea*. Palisades, N.Y.: Lamont-Doherty Geological Observatory, Columbia University.

Broecker, W., Lynch-Stieglitz, J., Archer, D., Hoffman, M., Maier-Reimer, E., Marchal, O., Stocker, T. and Gruber, N. 1999. How strong is the Harvardton-Bear constraint? *Global Biogeochemical Cycles* **13**(4), 817–820.

Cao, Y., Petzold, L. and Serban, R. 2003. Adjoint sensitivity analysis for differential-algebraic equations: the adjoint DAE system and its numerical solution. *SIAM J. Sci. Computing* **24**, 171–192.

Cessi, P. and Young, W. 1992. Multiple equilibria in two-dimensional thermohaline circulation. *J. Fluid Mech.* **241**, 291–309.

Dugdale, R. C. 1967. Nutrient limitation in the sea: dynamics, identification and significance. *Limnology and Oceanography* **12**, 685–695.

Falkowski, P., Barber, R. and Smetacek, V. 1988. Biogeochemical controls and feedbacks on ocean primary production. *Science* **281**, 200–206.

Francois, R., Altabet, M., Yu, E., Sigman, D., Bacon, M., Frank, M., Bohrman, G., Bareille, G. and Labeyrie, L. 1997. Contribution of Southern Ocean surface-water stratification to low atmospheric CO_2 concentrations during the last glacial period. *Nature* **389**, 929–935.

Garabato, A., Oliver, K., Watson, A. and Messias, M. 2004. Turbulent diapycnal mixing in the Nordic Seas. *Journal of Geophysical Research* **109**, C12010.

Gildor, H. and Tziperman, E. 2001. Physical mechanisms behind biogeochemical glacial-interglacial CO_2 variations. *Geophysical Research Letters* **27**, 3077–3080.

Griffies, S. and Tziperman, E. 1995. A linear thermohaline oscillator driven by stochastic atmospheric forcing. *Journal of Climate* **8**(10), 2440–2453.

Guilderson, T. P., Fairbanks, R. G. and Rubenstone, J. L. 1994. Tropical temperature variations since 20 000 years ago: Modulating interhemispheric climate change. *Science* **263**, 663–665.

Knox, F. and McElroy, M. 1984. Changes in atmospheric CO_2: Influence of marine biota at high latitude. *Journal of Geophysical Research* **89**(D3), 4629–4637.

Marotzke, J. and Willebrand, J. 1991. Equilibria of the global thermohaline circulation. *Journal of Physical Oceanography* **21**, 1372–1385.

Milliman, J. and Droxler, A. 1996. Neritic and pelagic carbonate sedimentation in the marine environment: Ignorance is no bliss. *Geol. Rundsch.* **85**, 496–504.

Milliman, J. and Troy, P. 1999. Biologically mediated dissolution of calcium carbonate above the chemical lysocline? *Deep Sea Res. I* **46**, 1653–1670.

Nilsson, J., Brostrom, G. and Walin, G. 2003. The thermohaline circulation and vertical mixing: does weaker density stratification give stronger overturning? *Journal of Physical Oceanography* **33**, 2781–2795.

Peacock, S., Lane, E. and Restrepo, J. M. 2006. A possible sequence of events for the generalized glacial-interglacial cycle. *Global Biogeochem. Cycles*, **20**, GB2010, doi: 10.1029/2005GB002448.

Polzin, K. L., Toole, J. M., Ledwell, J. R. and Schmitt, R. W. 1997. Spatial variability of turbulent mixing in the abyssal ocean. *Science* **276**, 93–96.

Restrepo, J. M., Leaf, G. K. and Griewank, A. 1998. Circumventing storage limitations in variational data assimilation. *SIAM Journal on Scientific Computing* **19**, 1586–1605.

Sarmiento, J. L. and Gruber, N. 2006. *Ocean Biogeochemical Dynamics*. Princeton University Press.

Sarmiento, J. L. and Toggweiler, J. R. 1984. A new model for the role of the oceans in determining atmospheric pCO_2. *Nature* **308**, 621–624.

Sarmiento, J. L., Dunne, J., Gnanadesikan, A., Matsumoto, K. and Slater, R. R. 2002. A new estimate of the *CaCO*3 to organic carbon export ratio. *Global Biogeochemical Cycles* **16**(4), doi:10.1029/2002GB001919.

Schmitz, W. 1995. On the interbasin-scale thermohaline circulation. *Reviews of Geophysics* **33**, 151–173.

Shaffer, G. and Olsen, S. 2001. Sensitivity of the thermohaline circulation and climate to ocean exchanges in a simple coupled model. *Climate Dynamics* **17**(5–6), 433–444.

Siegenthaler, U. and Wenk, T. 1984. Rapid atmospheric CO_2 variations and ocean circulation. *Nature* **308**, 624–626.

Stephens, B. and Keeling, R. 2000. The influence of Antarctic sea ice on glacial-interglacial CO_2 variations. *Nature* **404**, 171–174.

Stommel, H. 1961. Thermohaline convection with 2 stable regimes of flow. *Tellus* **13**(2), 92–96.

Takahashi, T. et al, 1999. Global air–sea flux of CO_2: An estimate based on measurements of sea-air pCO_2 difference. *Proceedings of the National Academy of Sciences of the United States of America* **94**(16), 8292–8299.

Thual, O. and McWilliams, J. C. 1992. The catastrophe structure of thermohaline convection in a two-dimensional fluid model and a comparison with low-order box models. *Geophysical and Astrophysical Fluid Dynamics* **64**, 67–95.

Toggweiler, J. R. 1999. Variations of atmospheric CO_2 by ventilation of the ocean's deepest water. *Paleoceanography* **5**, 571–588.

Toggweiler, J. R., Gnanadesikan, A., Carson, S., Murnane, R. and Sarmiento, J. L. 2003. Representation of the carbon cycle in box models and GCMs, part 1, the solubility pump. *Global Biogeochem. Cycles*, **17**(1), 1026, doi: 10.1029/2001GB001401, 2003.